UNIVERSITÀ DEGLI STUDI DI NAPOLI FEDERICO II
SCUOLA POLITECNICA E DELLE SCIENZE DI BASE

Doctorate in Earth, Environmental and Resources Science

~ XXX Cycle ~

PhD thesis

Geophysical investigation of the thermo-rheological state of Yellowstone Caldera

Advisor :

Prof. Maurizio Fedi

Co-Advisors:

Dr. Pietro Tizzani

Dr. Raffaele Castaldo

PhD candidate:

Mouna Brahmi

Coordinator of the Doctorate:

Prof. Maurizio Fedi

2017

Geophysical investigation of the thermo-rheological state of Yellowstone Caldera

A DISSERTATION

SUBMITTED TO THE EARTH, ENVIRONMENTAL, RESOURCES DEPARTMENT OF NAPLES UNIVERSITY, FEDERICO II IN A PARTIAL FULFILMENT OF THE REQUIREMENTS FOR THE DEGREE OF DOCTOR OF PHILOSOPHY

Mouna Brahmi

December 2017

Abstract

The thermal rheological state along with the depth to the Curie isothermal surface have been investigated in this thesis in order to provide a solid and a consistent subsurface image of the crust under Yellowstone caldera. This latter well-known caldera represents a unique geological and geophysical laboratory, where complex geodynamic processes in a continental hotspot are manifested, and it has been the center of interest for decades monitored since the fifties.

In the first part of this manuscript, I started by mapping the distribution of the depth to the Curie isothermal surface. To this end, I assume that the bottom of the magnetic crust corresponds to the depth of the iso-Curie surface where the magnetic minerals lose their magnetization due to the increase of temperature. Comparing with previous findings, our outcomes are computed with new aeromagnetic dataset with higher resolution, which play a key role in the improvement of the final results. I used two techniques based on spectral analysis of the magnetic anomalies: the first approach is the modified centroid method assuming a statistical ensemble of blocks of varying depth, width, thickness, and magnetization, each one uniformly distributed. It is simple to argue that this kind of distribution is not uncorrelated but it is instead a correlated distribution of magnetic sources, with a sloping exponent of about 3 that is within the fractal range. The misunderstanding may be explained in this way: even though the magnetization spectral factor is constant (a white power spectrum), the magnetization distribution must instead be defined by the product of spectral factors related to the prism size, magnetization and thickness, which is a red power spectrum, as discussed above. The second approach is the fractal distribution of magnetic sources, for which a spectral factor exists with a sloping exponent within the fractal range (from 2 to 4).

The application of the two methods to our dataset suggest that in both cases, a shallow Curie isothermal surface ranging from 1 km to 5 km is retrieved.

The second part of the thesis is focused on building a 3D thermal model. It was constructed through solving a 3D finite element problem of heat transfer in a conductive system using Comsol Multiphysics software involving a trial and error optimization of the density, velocity models jointly with the geothermal heat source parameters. The previous obtained depth to the Curie isothermal map was a key constraint parameter to check the validity of the thermal model.

Subsequently, a 3D rheological model was built using the 3D temperature model as an input along with the geological and the geophysical information from literature. The most part of earthquakes epicentres were found to be concentrated in the brittle zone of the volume while the

ductile zone is not totally homogeneous confirming the sandwich theory of the crust suggested by different authors which states that the ductile zone contains some brittle stratification. This brittle-ductile volume is the first 3D mapping of the rheological features of the crust under Yellowstone caldera.

The results obtained from this work can be considered as a new valuable information that provide a new insights into Yellowstone caldera, improve the monitoring of the volcanic evolution and assess the risk of its hazard.

Dedication

First of all, I dedicate this PhD thesis to my Grandmother "Khadhrouch" and to my dearest uncle "Farid", who cannot celebrate this achievement with me. I know you are in a better place, watching over me.

Second of all, every challenging work needs self-efforts as well as affection, love, encouragement of those who are close to our heart. This humble effort is dedicated to my sweet and loving parents

"Noura" & "AbdelFateh"

And to my backup team "Nada", "Wala" and "Chadha".

Finally, I would like to dedicate this thesis to all the people who kept me going when I wanted to give up, who believed in me and kept my life bright with their positive attitudes especially to "Imen" and "Chandra".

Acknowledgement

I would like to express my special appreciation and thanks to my advisor **Professor Maurizio Fedi**, you have been a tremendous mentor for me. I would like to thank you for encouraging my research and for allowing me to grow as a research scientist.

I am also grateful to my Co-Advisor, **Dr. Pietro Tizzani**, for his valuable suggestions and his permanent encouragements: I have been extremely lucky to have a supervisor like you who cared so much about my work, and who responded to my questions and queries so promptly. Thank you for pushing me to the edge without getting tired.

I extend my sincere acknowledgment to **Dr. Raffaele Castaldo** for spending his valuable time to correct my work. Your comments and suggestions helped me to improve the thesis.

I would like to express my gratitude and to recognize the effort of **Prof. Claire Bouligand.** She helped me a lot and she was more than patient with me. Thank you for taking the time to be more than advisor and to make my stay in **USGS** more enjoyable.

I also wish to thank **Dr. Farell** and **Dr. Huang** for their availability and how fast they provided the earthquakes data and the tomography data.

I am very grateful to **Dr. Youngmin Lee** from Korea Institute of Geoscience and Mineral Resources, South Korea for his help and his patience and to **Dr. Jacob B. Lowenstern** and **Dr. Shaul Hurwitz** from the United States Geological Survey for taking the time to sit and discuss my results with me.

I deeply thank the reviewers of the present study, **Prof. Maurizio Battaglia** and **Prof. Luca Di Siena**, for their insightful comments and encouragement.

A very genuine thank you is going to **Prof. Giovanni Florio** for his kind suggestions and willingness to answer all my questions. Special Thanks to **Prof. Federico Cella**, **Dr. Valeria Paoletti** and **Dr. Mahmoud Abbas** for their valuable advices.

Undertaking this PhD has been a truly life-changing and very challenging experience for me. During this PhD, I lost my Grandmother, my aunt and my uncle. I have been diagnosed with

Pneumothorax and I lost a part of my left lung. I had to overcome a lot of difficulties to get back to my normal life and finish what I already started. And all of this would never been possible without the support and guidance I received from many people. To all, I would like to say thank you for letting me enjoy every moment of my life in Naples.

Silvia, ***Monica*** and My Tunisian brother ***Davide***: Words cannot express how grateful I am for your presence in my life. They say: "the most memorable people in life will be the friends who loved you when you weren't very lovable" and you were more than just friends to me. You were my family and you will remain forever in my heart. You cannot imagine the feelings of love, gratitude and many more which I can't even explain neither can I state in a paragraph that I carry for each one of you. I simply adore and love each one of you. Thank you for being always there in my darkest and brightest moment.

Thank you **Mariem,** for being there for me. I don't believe that you will ever read this but I can't help but expressing my gratitude for your patience and kindness. Another special thank you to **Ibraheem,** you were there even in your worst situation and I am grateful. Both of you guys will be always in my heart.

Mimmo, no words can express how much I am grateful for your presence in my life. You made my stay in Naples easy and fun. Thank you.

I would especially thank my physician **Dr. Guggino Gianluca** for his availability, and also all the nurses, and all the nurse aids in the department of Chirurgia Toracica of Antonio Cardarelli hospital who made my stay less painful.

To all the people in **IREA**, who treated me like one of them and who were so kind to me during these three years: **Carlo, Simona, Manuela, Fabiana, Susy, Emanuela, Enzo, Riccardo, Ivana, Claudio, Nando, Carmen, Giuseppe, Adele, Pasquale, Michele, Mariarosaria, Antonio, Antonio, Giovanni and Diego** : Thank you.

A lot of people need to be thanked: people from my home country Tunisia, from Italy, from Germany, from India, from United States, from France and from China.

A big thank you to **Victoria, Randal, Jonathan, Anna, Maurizio, Hannah** and **Ashton** who opened their homes and hearts for me and who made my stay in US so exciting and so comfortable.

I would also like to thank all of my friends who supported and incented me to strive towards my goal: **Alessandro, Jirigalatu, Luca, Suchi, Giuseppe, Valentina, Emilie** and many others.

Last thank you is dedicated to all the people who walked out of my life. Thank you for showing me that true friends stick by your side and never stop caring about you. It made me appreciate what I have more and for that I am thankful.

At the end I would like to express appreciation to all my colleagues and friends: **Paoletta** my box-mate, **Andrea Vitale**, **Maurizio Milano** the sweets' sponsor, **Tina, Ivano, Dora, Shuang, Mahak** the real estate agent of the department , **Payal, Eleanora** and to everyone at the fourth floor of San. Marcellino.

I am blessed to have all of you in my life. Thank you for being part of my journey.

Table of Content

List of figures

List of Tables

Introduction

Calderas are geological structure associated with the collapse of the roof of the volcano magma chamber after a major explosion eruption. In particular, large Quaternary calderas (e.g., Yellowstone) are associated with the world's largest volcanic eruptions (Piskarev and Elkina., 2017). In this context, Yellowstone is one of the most spectacular and dangerous volcanoes on earth, and despite his long period of dormancy (now over 70.000 years), the caldera continuous to be an active and dynamic environment, with thousands of earthquakes, active ground deformation and considerable heat and mass flux. Therefore, studying its thermal behaviour and crustal status is very important to understand its future behaviour.

The aims of the present thesis are: (i) to investigate the thermal characteristics of the crust under Yellowstone by estimating the depth to the Curie isothermal and then, (ii) to evaluate the brittle ductile transition limit. The knowledge of the rheology and in particular the brittle-ductile (later referred as B/D) transition inside the crust and in the upper mantle may provide insights to verify the role of some geological mechanisms in the evolution of tectonic processes such as slab pull, crustal delamination and insurgence of volcanic process (Solaro et al., 2007).

The Curie isothermal surface is generally associated to a temperature reported in the bibliography as 570°C for magnetite (e.g. Bansal et al., 2011: 2013; Bouligand et al., 2009; Chiazzi et al., 2005; Dimri et al., 2000; Maus et al., 1997; Bhattacharyya and Le, 1975). An aeromagnetic survey (USGS, 2000) was used to investigate the depth to the Curie isothermal due to different reasons (i) a higher speed in collecting data, which implies lower costs and reduced effects on data of the magnetic field time variations; (ii) a better spatial coverage with respect to ground-based magnetic surveys, allowing surveying of areas inaccessible to ground work; (iii) a variable spatial resolution of the data as the flight altitude can be tuned to favour imaging of magnetic effects from structures of different sizes and depths.

The achieved cut-off of rock's magnetization surface, jointly with available geothermal information or/and the boreholes temperature (in our case, there are only very shallow and few boreholes temperature data for Yellowstone), and superficial heat flow measurements will allow us to constrain a thermal conductive model of the 3D temperature distribution in the upper crust under Yellowstone caldera, through an optimized finite element modeling.

More specifically, in order to investigate the thermal state of Yellowstone Caldera, we carry out a 3D time-dependent finite element model in a conductive thermal regime. The boundary settings considered for numerical model consist in the heterogeneous crustal domains determined by integration of a priori geological and geophysical information (Tizzani et al.,

2015). The initial condition will be determined by considering the major eruptive events of the volcanic area. Starting from the performed 3D thermal distribution, we will define the rheological stratification of the crust via the imaging of the B/D transition for the Yellowstone caldera area.

The B/D can be investigated via the rheological profiles that provide a representation of the mechanical strength of the crust (Ranalli, 1997). This approach is commonly used to correlate the thermo-mechanical structure of lithosphere with the seismicity or active ground deformation in a wide variety of geodynamic environments.

To this purpose, I constrain the rheological crust models by using the information derived by thermal investigation of the area (i.e. geothermal and heat flow measurements) and data derived from an aeromagnetic survey measurements. In particular, I focus my attention to the inversion of the available aeromagnetic data in order to individuate the Curie isothermal depth surface. That is the crustal depth where after it, the crustal rocks lose their magnetic field due to inverse temperature.

This present manuscript starts with an introduction where I explain the motivations behind this work, an overview of the methodologies used and the expected results. Chapter 2 is a geological review of Yellowstone National Park area: I collected the most important information about Yellowstone plateau seismicity and crustal structure and the volcanic system of that area. The most important concepts behind the magnetic field and the rheology are explained in Chapter 3, it contains the necessary tools to understand the main two chapters of this thesis. The estimation of the depth to the Curie isothermal is discussed in Chapter 4, where I used two different spectral analysis methods: the modified centroid method and the fractal analysis method. In Chapter 5, I built the 3D thermal model and the 3D rheological model and we constrain the result with the available surface heat flow measurements and the acquired depth to the Curie isothermal from Chap.3. Finally, some conclusions are given and some future perspectives are recommended.

Chapter 2: Geological Framework

2.1. Geological Setting

The so-called Yellowstone Plateau covers an area of about 6,500 km^2, mostly within the Yellowstone National Park, which extends from northwestern Wyoming, northeastern Idaho and southern Montana (USA). The Yellowstone Plateau is one of the largest latest Pliocene and Quaternary silicic volcanic fields on Earth with an original extent of almost 17,000 km^2 (Hilderth et al., 1984). The geologic history of the field defines three cycles of volcanic events which have erupted more than 6,000 km^3 and have been characterized by the eruption of extensive sheets of rhyolitic ash-flow tuff interrupted by eruptions of rhyolitic lavas and tuffs in and near the source areas of the ash-flow sheets and by the eruption of basalts around the margins of major rhyolitic volcanism (Christiansen, 2001).

Based on secular geochemical and isotopic relations and eruptive histories (e.g. Hildreth et al. 1984, 1991; Christiansen, 2001; Vazquez and Reid, 2002), each cycle has been interpreted as the result of the accumulation, storage, and differentiation of discrete silicic magma reservoirs (Figure 1):

- The rocks of the oldest cycle erupted between about 2.2 and 2.1 Ma, are basalts in northern and eastern Yellowstone National Park and a rhyolitic lava flow at the south end of Island Park, Idaho. The oldest ash-flow sheet of the Yellowstone Group, the Huckleberry Ridge Tuff, was erupted at 2.1 Ma and was emplaced as a single cooling unit of more than 2,450 km^3 over an area of 15,500 km^2.
- The second cycle: Rocks of this cycle are present just west of Yellowstone National Park and probably are buried beneath the Yellowstone Plateau. Early second-cycle rhyolite flows crop out west of Island Park. The Mesa Falls Tuff, exposed near Island Park, is a cooling unit of more than 280 km^3, erupted at 1.3 Ma within the northwestern part of the first-cycle caldera.
- The third cycle perhaps overlapped the second, beginning about 1.2 Ma with eruption of rhyolitic lavas and related tuffs around a growing annular fissure system encircling central Yellowstone National Park. Flows vented periodically along this fissure system for about 600,000 years until ring-fracture development was terminated by rapid emplacement of the ~1,000 km^3 ash-flow eruptions of the Lava Creek Tuff at at 639±2 ka (Lanphere et al. 2002), probably through the same ring-fracture zone. These ash flows buried more than 7,500 km^2. The floor of Yellowstone caldera has been subsequently filled by rhyolite lavas and lesser tuffs primarily composing the Upper Basin and Central Plateau Members of the Plateau Rhyolite (Christiansen and Blank 1972).

Each sequence of volcanism resulted in the collapse of a central area and while the oldest two calderas are no longer visible because are buried beneath younger basaltic lava flows and sediments that blanket the Snake River Plain, the latest caldera covers an area 60 km wide and 40 km long.

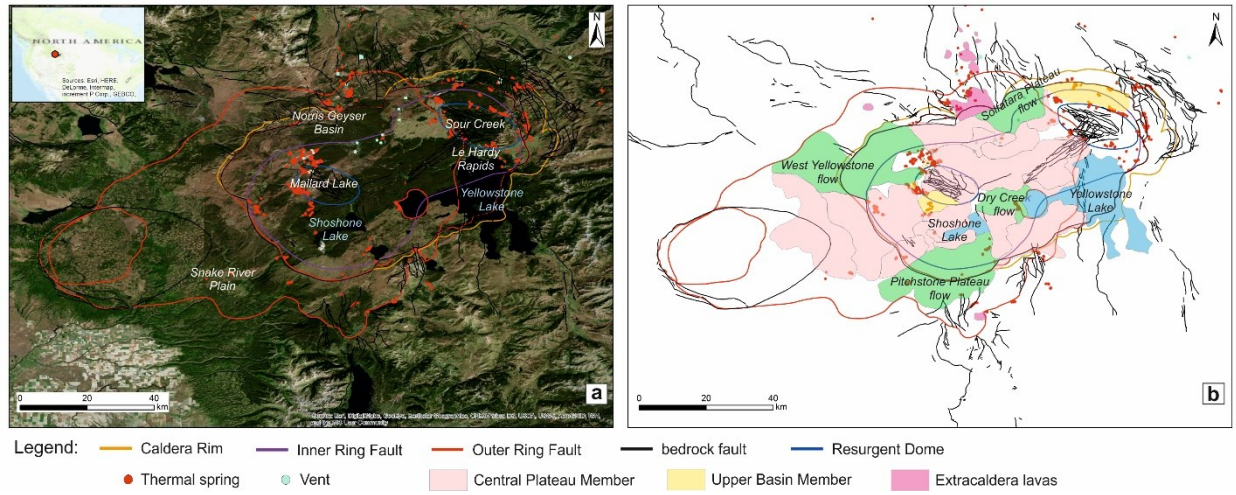

Figure 1. Yellowstone caldera (a) and associated Plateau Rhyolite lavas and tuffs (b) (modified from Vazquez and Reid, 2002). Data available from the Wyoming State Geological Survey and U.S. Geological Survey.

2.2. Ground deformation in Yellowstone's Volcanic System

Since the last eruption (about 70,000 years ago), Yellowstone has remained restless, with high seismicity and continuous uplift/subsidence episodes. Furthermore, the widespread hydrothermal system with over 10,000 geysers hot springs, and fumarole of Yellowstone National Park indicates that the underlying volcanic system remains active. To entirely understand the volcano's behavior and forewarn a potential reawakening, a volcano surveillance center for monitoring Yellowstone's activity was specifically created in 2001, complementing existing ones for Hawaii, Alaska, the Cascades, and Long Valley, California. The Yellowstone Volcano Observatory (YVO) is supported jointly by the U.S. Geological Survey, the University of Utah, and Yellowstone National Park.

The monitoring activity currently includes different types of observations on a continuous or near-real-time basis: earthquakes, ground movement, volcanic gas, rock chemistry, water chemistry, remote satellite analysis (Figure 2). By integrating previous data with the latest technological resources, scientists have been able to track in time rapid uplift and subsidence of the ground connected with significant changes in hydrothermal features and earthquake activity (Evans et al., 2010; Farrell et al., 2010). Benchmarks surveys discovered an unprecedented uplift of the Yellowstone Caldera of more than 72 cm over five decades during the period 1923-1975

(Pelton and Smith, 1982), especially in the east-central part of the Yellowstone caldera, near the base of Mallard Lake and the Sour Creek resurgent dome where an average rate of 14±1 mm/year from 1923 to 1976 and 22±1 mm/year from 1976 to 1984 were recorded (Dzurisin et al., 1994). The uplift was associated to the influx of molten material into the upper crust beneath the caldera (<20km of depth).

Additional surveys across the eastern part of the caldera nearly every year have been conducted from 1983 to 1998. The new findings revealed a nearly continuous movement in time but with a different trend. The floor of the caldera continued to rise until 1984, stopped rising during 1984-85, and then subsided for the following 10 years at rates of 19 mm/yr (Dzurisin et al., 1994; Wicks et al., 1998; Stauffer, 2004). The earthquake swarm of late 1985 may have been caused by the escape of hydrothermal fluids through the impermeable rock layer above the magma reservoir, which also initiated the episode of subsidence in the caldera.

Starting from 1987, GPS was added to the Yellowstone monitoring system and corroborated the results from the leveling surveys (Meertens, et al., 1991) and several years later new and revolutionary satellite-based method - Interferometric Synthetic Aperture Radar (InSAR) - has been deployed in order to assemble a more detailed picture of how and when the ground moves above Yellowstone's magma reservoir.

Until the 1990s, it was thought that all the inflations and deflations was located near Le Hardy Rapids, in the central part of the caldera which began rising again in 1995, but a more complex pattern of uplift and subsidence has prevailed since 2000. InSAR data show that between 1995 and 1997 a large area along the northwest rim of the Yellowstone Caldera, centered near Norris Geyser Basin, started to rise. A period of uplift of 12 cm, between 1997 and 2003, in the northern part of the Yellowstone caldera connected with pulse of basaltic magma (Wicks, et al., 2006). Since that time, the area, including the Norris Geyser Basin, has stopped moving, while uplift has returned to the central part of the caldera and the two resurgent domes and along the Northern Caldera Rim. In particular, geodetic measurements of Yellowstone ground deformation from 2006 to June 2010 reveal deceleration of the recent uplift of the Yellowstone caldera following an unprecedented period of uplift that began in 2004. In 2006–2008 uplift rates decreased from 7 to 5 cm/yr and 4 to 2 cm/yr in the northern and southwest caldera, respectively, and in 2009 rates further reduced to 2 cm/yr and 0.5 cm/yr in the same areas (Chang et al., 2010).

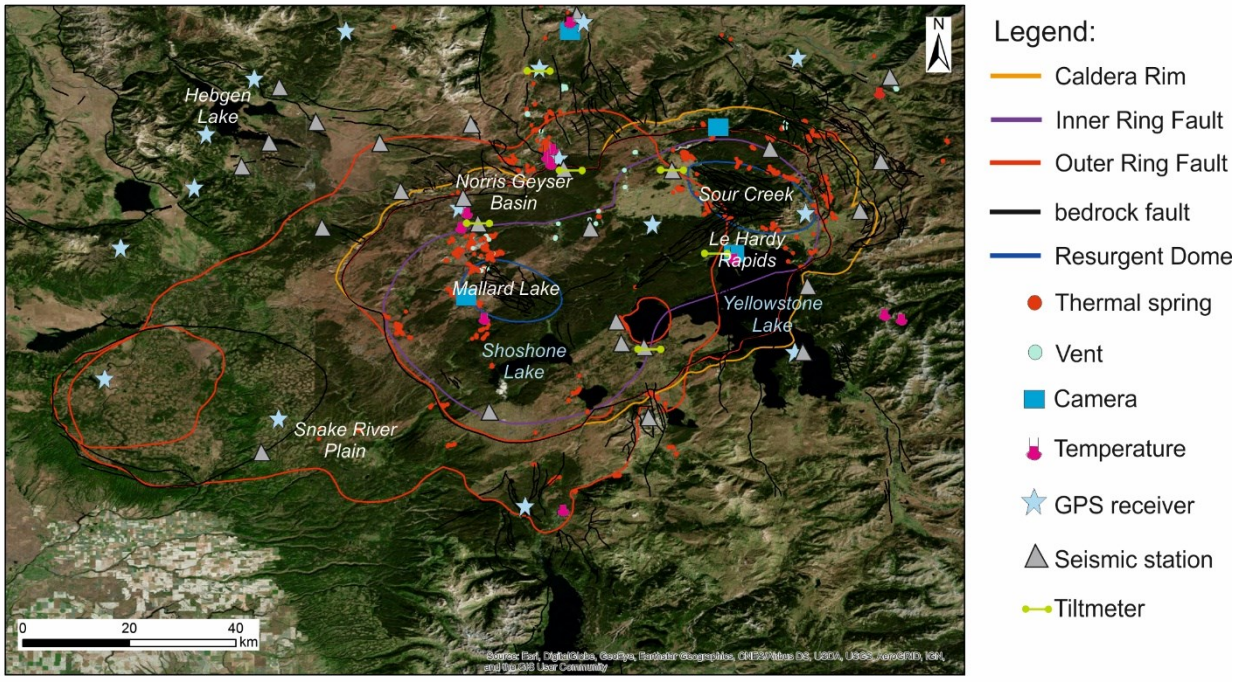

Figure 2. Monitoring instruments of the YVO in the Yellowstone Caldera (available at https://volcanoes.usgs.gov/volcanoes/yellowstone/monitoring_map.html).

2.3. Yellowstone Plateau seismicity

The Yellowstone region is one of the most seismically active areas of the western U.S. with often 1 to 20 earthquakes recorded everyday which amount to over a thousand earthquakes per years (Waite and Smith, 2004). Historical seismicity of Yellowstone (Figure 3), monitored since the installation of a permanent seismic network in 1973, is distinguished by spatial and temporal clusters of small and shallow earthquakes (<5 km depth). About 40% of the total earthquakes are associated with swarms, most of which have magnitudes less than 4 and concentrates between the 0.64 Ma northern rim of the Yellowstone caldera and the 44-km-long rupture of the 1959 M_S7.5 Hebgen Lake earthquake (the largest historic earthquake in the western U.S. interior) where the cumulative seismic moment release in this region is an order of magnitude higher than inside the Yellowstone caldera, implying the dominance of aseismic mechanisms for the caldera (Puskas et al., 2007). The central part of the caldera has relatively low seismicity, and no distinct seismic patterns are associated with the Mallard Lake or the Sour Creek resurgent domes.

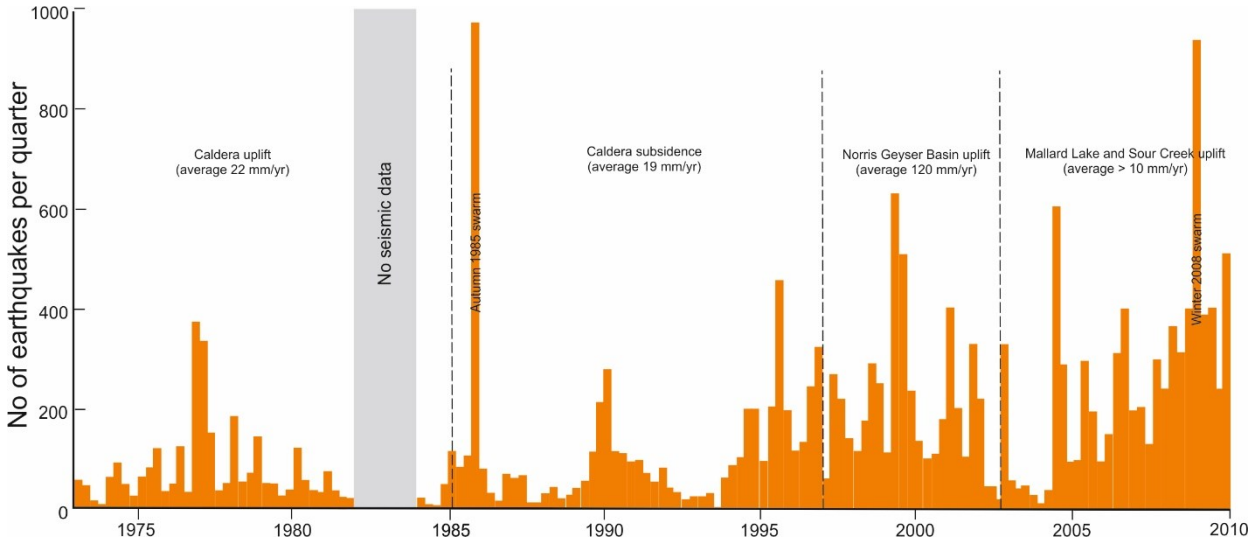

Figure 3. - Plot of recorded earthquake activity with a minimum magnitude cutoff of MC 1.5 at Yellowstone from 1974 through 2010 along with caldera crustal deformation (modified from Waite and Smith, 2002). Data available from U.S. Geological Survey.

Focal mechanisms reveal predominantly normal faulting. However, fault orientations vary across the Yellowstone caldera. Furthermore, events do not always occur along the mapped and dated Late Quaternary faults such as the Hebgen, Madison, and Gallatin faults (Smith and Arabasz, 1991; Miller and Smith, 1999), as many seismogenic structures may have been buried by the post-caldera rhyolite flows and yet still act as zones of weakness (Christiansen, 2001).

The picture that emerges from all these data is of a dynamic system in which the caldera floor is in almost constant motion with episodes of uplift and subsidence occurring at various locations and over different time scales. Spatial and temporal variations of Yellowstone ground movement are correlated with changes in seismic and hydrothermal activity in and around the caldera (Waite and Smith, 2002, Chang et al., 2007, Smith et al., 2009).

2.4. Yellowstone Plateau crustal structure

Earliest works on the structure of the Yellowstone volcanic system included earthquake and Curie isothermal depth determinations that revealed a shallow crustal heat source and focal mechanisms consistent with general crustal extension of the Yellowstone Plateau (Smith et al., 1974, 1977). Controlled source seismic studies revealed a relatively homogenous lower crust to 40 km deep that was similar to that of the surrounding lithosphere not affected by lower crustal magmatism but could not discern the shape or depth of low velocity upper crustal source (Smith et al., 1982; Schilly et al., 1982; Lehman et al., 1982). This seismic image of the magma reservoir is consistent with a geochemical model by Lowenstern and Hurwitz (2008) that suggests magma

rises closest to the surface (5–7 km depth) beneath the resurgent domes. Their model, based on CO^2 flux and heat flow, requires continued intrusion of plume-derived basalt to sustain the silicic, upper-crustal magmatic system responsible for Yellowstone's youthful volcanism.

New findings have been possible in the latest 30 years thanks to the inversion of GPS and/or InSAR and/or leveling correlated with gravity measurements and seismic tomography studies. The new datasets provide important constraints on the dynamics of the Yellowstone magma system and its potential for future volcanic eruptions and earthquakes.

The findings can be summarized in two families of models which have been proposed to explain surface deformation at Yellowstone Caldera (Tizzani et al., 2015): "hydrothermal" or "magmatic" model.

The former relies mainly on pressurization/depressurization of fluids other than magma to produce surface uplift/subsidence. The primary deformation mechanism is a pressure change within the hydrothermal system in response to some perturbation such as a gas/fluid pulse where:

- According to Fournier (1989), the inflation episodes are given by phase separation from crystallizing magma and trapped beneath a self-sealing layer at lithostatic pressure in ductile rock and rupturing of the seal would produce subsidence
- Another theory invokes the poroelastic deformation in the shallow hydrothermal system induced by magmatic gas influx at the base of the hydrothermal system (Dzurisin et al., 1999; Hutnak et al., 2009)

In any of the two hydrothermal representations, the model implies that the depth of the sources should be above the brittle-ductile transition zone, that in Yellowstone is at a depth between 4 and 6 km under the resurgent domes area (DeNosaquo et al., 2009), and that their density should be $\rho \leq 1000$ kg/m^3.

Differently, the primary deformation mechanism associated with the magmatic models is the injection of magma or fluid exsolved from magma at or below the base of the hydrothermal system at depth below the brittle-ductile transition zone and density around 2500 kg/m^3.

In this framework, tabular bodies beneath the caldera have been identified as the source of deformation which have been intermittently active during the last three decades: (1) one (e.g., Chang et al., 2007; Farrell et al., 2014) or two (e.g., Wicks et al., 2006) bodies at a depth of 6-14 km beneath the caldera resurgent domes and (2) a source 8-16 km deep under the Northern Caldera Rim area. The microgravity observations by Arnet et al. (1997) are consistent with a "magmatic" model where surface uplift is caused, at least in part, by intrusion of magma in the

midcrust, while subsidence could either be the result of fluids migration outside the caldera or the gravitational adjustment of the source from a spherical to a sill-like geometry (Tizzani et al.,. 2015). The source depths indicated by these models are below the brittle-ductile transition-thought to occur at a depth between 4 and 6 km under the resurgent domes area (DeNosaquo et al., 2009).

Chapter 3: Introduction to Magnetic and Rheology

3.1. Magnetic field

3.1.1. Earth's Magnetic Field

Our planet is surrounded by a magnetic field, which, similarly to the gravity field, admits a scalar potential and can be measured by magnetic instrumentation. The geomagnetic field is approximately dipolar with a dipole axis inclination of about 10.3° from the Earth's rotation axis. However, the signal obtained from magnetic field measurements is a sum of different source contributions which may be summarized in three main categories:

- The main field, generated in the Earth's fluid core by a geodynamo mechanism;
- The lithospheric field, generated by magnetized rocks in the Earth's lithosphere;
- The external field, produced by electric currents in the ionosphere and in the magnetosphere, due to the interaction of the solar electromagnetic radiation and the solar wind with the Earth's magnetic field.

Moreover, the Earth's magnetic field structure varies not only in a spatial scale but is also subject to continuous long-term and short-term time variations. The long-term variations (secular variations) have deep origin and may be detected by the use of datasets covering large periods of time (at least 5-10 years), while the short-term variations have external origin and generally cover very short range of time (from second to few years) (Lanza and Meloni, 2006).

In this brief overview, we are going to talk about the lithospheric component of the magnetic field since we are interested to retrieve the properties of magnetic source in the Earth's crust. Many authors studied the magnetic contribution in the uppermost mantle, at least in a specific geological environments (e.g. Arkani-Hamed and Strangway, 1987; Bostock et al., 2002; Blakely et al., 2005; Chiozzi et al., 2005; Ferré et al., 2014).

1.1.1. The lithospheric magnetic field

In the space exterior to the Earth's surface, assuming the absence of magnetic material, Maxwell's equations are expressed in SI units as:

$$\nabla \cdot \mathbf{B} = 0 \quad (1.1)$$

$$\nabla \times \mathbf{B} = \mu_0 \mathbf{J} \quad (1.2)$$

Where **B** is called magnetic induction or flux density. It is measured in Tesla (T) or nano-Tesla (nT), more conveniently in the geomagnetic field studies; **J** is the current density in Ampere per square meter (A/m^2), and μ_o, known as the permeability of free space, is a constant equal to $4\pi \times 10^{-7}$ henrys per meter (H/m) (Blakely, 1996).

Then, if $\nabla \times \mathbf{B} = 0$, we have that:

$$\boldsymbol{B} = -\nabla \Psi \quad (1.3)$$

Where Ψ is the magnetic potential.

So, substituting (1.10) in (1.8), we will obtain:

$$\nabla^2 \Psi = 0 \quad (1.4)$$

That is, the potential satisfies Laplace's equation.

So, the magnetic field measured at a specific position r and time t may be defined as:

$$\mathbf{B}(\mathbf{r}, t) = \mathbf{B}_m(\mathbf{r}, t) + \mathbf{L}(\mathbf{r}) + \mathbf{D}(\mathbf{r}, t) + \mathbf{e}(t), \quad (1.5)$$

Where $\mathbf{B}_m(\mathbf{r}, t)$ is the field produced by the Earth's core (main field), **L**(**r**) is the lithospheric field, **D** (**r**,*t*) the external field and **e**(*t*) the measurement error. By this, the lithospheric or external residual field may be obtained subtracting the main field to the magnetic measurement.The description of the core magnetic field is referred to a model, called International Geomagnetic Reference Field (IGRF), which is updated every five years by IAGA (International Association of Geomagnetism and Aeronomy) due to time variations of the geomagnetic field.

The solution of Laplace's equation expressed in a spherical harmonic representation provides a formal separation of the internal ($\mathbf{B_m} + \mathbf{L}$) and external (**D**) field components. In fact, each source region is defined by specific spherical harmonic terms (degree l and order m), which determine the spatial scale of such contribution. Generally, low degrees correspond to the largest spatial scales, or to the deepest source contributions, and vice-versa. This representation was used by Gauss in the 19th century to fit the magnetic observatory data and show that the largest part of the geomagnetic field is by far of internal origin.

3.1.2. Magnetic properties of the rocks

The origin of the lithospheric fields is strictly related to the magnetic properties of the rocks within the crust, which vary for different geographical regions, mineral composition and temperature. The magnetic effect on materials allows identifying three different categories (Reynolds, 1977):

- Diamagnetic materials have a weak, negative susceptibility to magnetic fields.
- Paramagnetic materials have a small, positive susceptibility to magnetic fields.

These materials are slightly attracted by a magnetic field and the material does not retain the magnetic properties when the external field is removed.

- Ferromagnetic materials have a large, positive susceptibility to an external magnetic field. They exhibit a strong attraction to magnetic fields and are able to retain their magnetic properties after the external field has been removed.

For understanding the behavior of rocks materials in a magnetic field environment, we may start defining **m** as the magnetic moment of a simple dipole, expressed in [$A\ m^2$], which leads to the magnetization (**M**) in the case of a large volume (V) composed of several single dipoles :

$$\mathbf{M} = \frac{\sum_i \mathbf{m_i}}{V} \quad (1.6)$$

Where $\mathbf{M}$ is measured in A/m.

Then, we may rewrite the Maxwell's equation to obtain the magnetization current $\mathbf{J_m}$:

$$\nabla \times (\mathbf{B} - \mu_0\, \mathbf{M}) = \mu_0\, \mathbf{J} \quad (1.7)$$

And we define the magnetic field intensity **H** as:

$$\mathbf{H} = \frac{\mathbf{B} - \mu_0 \mathbf{M}}{\mu_0} \quad (1.8)$$

M and **H** are related by the magnetic susceptibility (χ), which determines the ease with which a material is magnetized:

$$\mathbf{M} = \chi \mathbf{H} \quad (1.9)$$

So, the magnetic field expression becomes:

$$\mathbf{B} = \mu_0(\chi + 1)\mathbf{H} = \mu \mathbf{H} \quad (1.10)$$

Where, μ is the absolute permeability.

Here we mean that the magnetization is induced ($\mathbf{M_i}$) by the external field $\mathbf{H}$, there is also a component of the magnetization which is called permanent or remanent ($\mathbf{M_r}$). In crustal materials, remanent magnetization is a function not only of the atomic, crystallographic, and chemical make-up of the rocks, but also of their geologic, tectonic, and thermal history (Blakely, 1996). So, the rock magnetization may be written as:

$$\mathbf{M} = \mathbf{M}_i + \mathbf{M}_r \quad (1.11)$$

From which we obtain the Koenigsberger ratio(Q):

$$Q = \frac{|\mathbf{M}_r|}{|\mathbf{M}_i|} = \frac{|\mathbf{M}_r|}{\chi|\mathbf{H}|} \quad (1.12)$$

Both magnetizations arise from spontaneous magnetization, a complex property of the ferromagnetic minerals in the Earth's crust. The spontaneous magnetization is dependent on the temperature. As a material is heated, the spacing between neighboring atomic moments increases to a threshold point where the spontaneous magnetization falls to zero. This temperature is called the Curie isotherm, whose definition is discussed in more detail in Chapter 4. Hence, both induced and remanent magnetizations vanish at temperatures greater than the Curie isotherm. Paramagnetic and diamagnetic effects persist at these temperatures, but from the perspective of magnetic-anomaly studies we may consider rocks above the Curie isotherm to be nonmagnetic. The Curie isotherm differs for each mineral formation but, in magnetic field studies, the Curie isotherm of Magnetite (about 580°C) is considered as the standard temperature boundary for the whole magnetic crust with magnetite as the main magnetic mineral for percentage, size, and shape (Hunt et al., 1995).

3.1.3. Investigation of the depth to the Curie isotherm (CD) in literature

The Curie isotherm was named after Pierre Curie, who showed that magnetism was lost at a critical temperature. This temperature is assumed to be 580 °C for magnetite, which is the dominant magnetic mineral in the deep crust within the continental region (Langel and Hinze, 1998), at atmospheric pressure. The Curie depth (CD) at which temperature reach the Curie point is assumed to be the bottom of the magnetized bodies in the earth crust (Khojamli et al., 2016), bellow that the lithosphere is vertically nonmagnetic.

The depth to Curie isotherm can also provide an understanding of the thermal structure: e.g., in volcanic areas convective heat transfer complicates the determination of the thermal structure from heat flow measurements alone and determination of Curie isotherm point depths from magnetic data can prove to be helpful for understanding the thermal structure (Mita Rajaram., 2007).

The remotely sensed magnetic (surface, airborne, satellite-borne) measurements indirectly provide an isothermal surface within the lower crust. The first use of the aeromagnetic data was dated to 1975 where Bhattacharyya and Leu (1975), mapped for the first time the CD for geothermal reconnaissance in Yellowstone National Park in USA and their results were balancing between 4and 8 km of depth. In Greece and from aeromagnetic and heat flow data, Tselentis (1991) was able to understand the nature and the extent of the regional geothermal system through constructing the Curie isotherms which varies considerably, reaching 20 km towards western Greece and about 10 km beneath the Aegean. In east and Southeast Asia, Tanaka et al. (1999) determined the CD using the spectral analysis of magnetic anomaly method; they estimated the CD in that area, using the centroid method and many heat flow boreholes, to be ranging from 9 to 46 km which was pretty close to the result from the heat flow data. Dolmaz et al., (2005) conducted a study of the relationship between the earth crust's thermal structure in the southwestern and the study of the brittle ductile transition in that area as well as the heat flow variations.

Curie isotherm varies from region to region depending on the geology and the mineralogical content of the rocks. Therefore, one can normally expect shallow Curie point depth at the regions, which have geothermal potential, young volcanisms and thin crust (Aydin and Oksum 2010). The assessment of the variations in the Curie isotherm depth of an area can provide valuable information about the regional temperature distribution at depth and the potential of subsurface geothermal energy (Tselentis 1991) as well as the geothermal gradients of the region.

Combining a travel time inversion of a micro-seismic dataset together with a CD analysis based on aeromagnetic data allowed Karastathis et al. (2010) to found the deep origin of the geothermal fields and volcanic centers in central Greece, they estimated the CD at about 7 to 8 km.

The aeromagnetic data was used also by Bansal et al., (2011) in order to estimate the CD in Germany: using the centroid method and comparing the results with the heat flow density data. Salah et al. (2013) estimated the CD of the Northern Red Sea rift in Egypt using the spectral analysis of the aeromagnetic data: the result varied from 5 to 20 km. The shallowest depths of 5 km are associated with a high heat flow and suggested a promising area for geothermal exploration.

In the Eastern sector of central Nigeria, Eletta and Udensi (2012) investigated the CD isotherm from aeromagnetic data to prepare a preliminary potential map of geothermal resources. They showed that the high prospect areas are located in the south-west parts of the study area, whereas applying the spectral analysis of aeromagnetic data for geothermal prospecting in the north-east of Nigeria was conducted by Obande et al. (2014), they estimated the top and the centroid depths of magnetic sources from the power spectrum and they obtained results that varies from 6 km near the thermal springs to 12 km elsewhere.

From a magnetic analysis of the Tohoku arc, Japan, Okubo, and Matsunaga (1997) find that the CD varies from 10 km in the volcanic province of the back arc to 20 km or deeper at the eastern limit of Tohoku. They find that the boundary between the seismic and aseismic zones in the overriding plate correlates with the inferred Curie isotherm, indicating that the seismicity in the overriding plate is related to temperature.

3.2. Rheology

Rheology is the science dealing with the deformation and flow of matter. Shear stress, shear rate and viscosity are the building parameters leading to an understanding of rheology. Viscosity is a measure of a fluid's resistance to flow. When, a fluid starts to flow under the action of a force, a shearing stress arises everywhere in that fluid that tends to oppose the motion. As one layer of the fluid moves past an adjacent layer, the fluid's molecules interact so as to transmit momentum from the faster layer to the slower layer trending to resist the relative motion. The intent of this part is to explain the fundamentals of rheology since we are going to use it in the second part of this thesis.

The distinguishing feature of a fluid, in contrast to a solid, is the ease which the fluid may be deformed. If a shearing force, however small, is applied to a fluid, the fluid will move and continue to move as long as the force acts on it. Even though a fluid can deform easily under an applied force, the fluid's viscosity creates resistance to this force. Here are some simple definitions of some terminology used while studying the rheology of a field in order to provide some basic understanding of the field.

3.2.1. Viscosity

In a very simple way, viscosity is the resistance measure of a fluid to an applied stress. Sir Isaak Newton was the first to define viscosity. Newton assumed the force required to maintain a difference in speed was proportional to the difference in speed through a liquid. This simple relationship in fluids for which the shear stress divided by the shear rate (which remain equal independent of the shear rate in case of Newtonian fluid) is the practical definition of viscosity.

The viscosity depends on the shear rate, temperature, pressure, time (the history of the shear) and the physical properties of the media.

3.2.2. Shear stress

Shear stresses is a stress that causes shear. It is of the same dimension as pressure. But while pressure causes compression, shear stresses cause shear. It tends to deform the material without changing its volume, and are resistant to the body's shear modulus. In other words, it means the load resisted by the section of a material taken parallel to the external load direction. Whenever an external load is applied on a member, the load tends to deform the body in turn the resisting forces are developed in the member to counteract the deformations, this resisting force developed per unit area of the section of the material is called stress.

Shear stress produces shear deformation in form of angle. So here the proportionality constant is Modulus of rigidity (G), as in case of stress produces strain where the proportionality constant is Young's modulus of elasticity (E). When there is only normal stress acting on a body then there is no shear stress as only linear deformation will be there, however normally every materials subjected to biaxial or triaxle stress system where shear stress at different plane exists. The shear deformation angle plays an important peat while analyzing failure of any materials.

3.2.3. Shear Rate

Velocity change in the field where the fluid flows over an adjoining layer. It defines the term of viscosity which is the resistance to movement of fluid (a definition for Fluid Mechanics) For example: Non-Newtonian Models.

For the Non Newtonian, fluids tend to be the rule rather than the exception in the real world, making an appreciation of the effects of shear rate a necessary for anyone engaged in the practical application of rheological data. It would, for example, be disastrous to try to pump a dilatant fluid through a system, only to have to go to solid inside the pump, bringing the whole process to an abrupt halt. While this is an extreme example, the importance of shear rate effects should not be underestimated. When a material is to be subjected to a variety of shear rates in processing or use, it is essential to know its viscosity at the projected shear rate. If these are not known, an estimate should be made.

Chapter 4: Estimation of the depth to the Curie isothermal surface in Yellowstone

4.1.Introduction

Yellowstone National Park (YNP), located in the northwest of Wyoming, is considered a significant geothermal energy source. Many authors studied its geothermal flow using different kind of data (e.g. Lowenstern and Hurwitz, 2008; Vaughan et al., 2012; Hurwitz and Lowenstern, 2014). Vaughan et al. (2012) used ASTER, a NASA satellite, to estimate how much geothermal heat was radiating away from Yellowstone thermal area, which was about 1,970 megawatts. Most of the heat flow studies (e.g. White, 1969; Ellis and Wilson, 1955; Fournier et al., 1976; Hurwitz et al., 2007; Lowenstern and Hurwitz, 2008; Vaughan et al., 2012; Hurwitz and Lowenstern, 2014) were conducted on Yellowstone thermal features: thermal springs, mud pots, geysers, and still the heat flow remains poorly known in our study area. In order to provide an independent estimation of the thermal status of Yellowstone, I investigate the depth to the Curie isothermal surface in the area using aeromagnetic data and through two different methods based on spectral analysis technique. The Curie isotherm is about 570°C, which represents the bottom of magnetic sources. In other words, it is when materials tend to lose their magnetic properties and become paramagnetic (e.g. Langel and Hinze, 1998; Rajaram, 2007).

Surprisingly, the only extensive published study of the depth to the Curie isothermal surface in Yellowstone caldera, was done back in 1975 by Bhattacharyya and Leu (Bhattacharyya and Leu, 1975) using aeromagnetic data from a survey conducted over Yellowstone in 1973.

It is important to mention that the depth to the Curie isotherm surface in Yellowstone area was estimated before Bhattacharyya and Leu (1975) by Shuey et al. (1973) and Smith et al. (1974) who studied the average isotherm depth for the whole area.

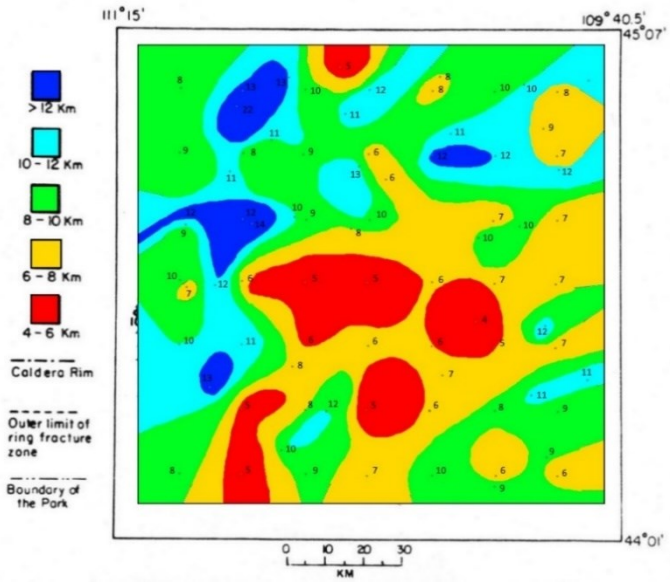

Figure 4. Estimation to the depth to the Curie isotherm surface in Yellowstone after Bhattacharyya and Leu., 1975

The results of Bhattacharyya and Leu (1975) are shown in Figure 4. The authors used the centroid method developed by Spector and Grant (1970) to estimate the Curie depth and they concluded that the central area of the caldera was marked by a shallow Curie isotherm at depths of only 5 to 6 km whereas, the isotherm outside (but within the caldera rim) lied generally at depths of 6 to 8 km. They also mentioned that, around the south-eastern and the southern sections of the study area, there were some significantly shallow depths ranging from 4 to 6 km which could indicate the presence of local hot spots.

In this present study, I am going to use both spectral analysis approaches: fractal (Maus et al., 1997) and the corrected Spector and Grant (1970) method (Fedi et al., 1997), which is defined in the whole chapter as the modified centroid method. First I will present the aeromagnetic data used in this work. Then, I will explain the two methods employed to estimate the depth to the iso-Curie surface. Finally, I will interpret and discuss the results.

4.2. Data

In this study, I am going to use the aeromagnetic data collected over YNP from the aeromagnetic survey conducted in 1997 (USGS, 2000): the survey, named Yellowstone 97, covers about 106 km by 112 km. It was flown between September and October 1997 in an east- west direction with an averaged altitude of 244 m relative to sea level. The line space used is about 400 m.

The survey (U.S. Geological Survey, 1973) used by Bhattacharyya and Leu (1975), covers 131 km by 131 km, was flown with an elevation of about 4 km above YNP. The advantage of using a single survey is that we have a coverage of our study area with a homogeneous flight spacing and flight elevation with high resolution. Some studies (e.g. Bouligand et al., 2009) tend to overlap different surveys to cover a larger area of study.

The major limitation of this survey is the area size: an area of 106 km by 112 km is considered small comparing to different areas and can cause some errors during computations. The Yellowstone 97 allows us to have a high resolution data with short wavelength magnetic anomalies (Grauch and Millegan., 1998). The aeromagnetic map (Figure 5), is a residual magnetic map of just Yellowstone area obtained from an open file with the U.S. Geological Survey. It was gridded using Oasis software using the minimum curvature gridding technique with a step of 200 m. They had already removed the Earth's main geomagnetic field without being Reduced to the Pole, although Finn and Morgan (2002) later have reduced the data to the North Pole.

The principal feature noted in the map (Figure 5) is the high magnetic intensity, which reaches 250 (nT) in the northeast part of Yellowstone. This part corresponds to the Absaroka Mountains in the geological map (Figure 6). The lowest magnetization (-375 nT) is located in the caldera area (Figure 5) which can be explained by the topographically low area accompanied by hydrothermally altered volcanic rocks (Figure 6). It can be also explained by the fact that the igneous rocks in the caldera reserved their magnetization or it can be the result of the absence of magnetic rocks (Finn and Morgan, 2002). The presence of a good correlation between the aeromagnetic map of Yellowstone and its geological and the topographic map is clear.

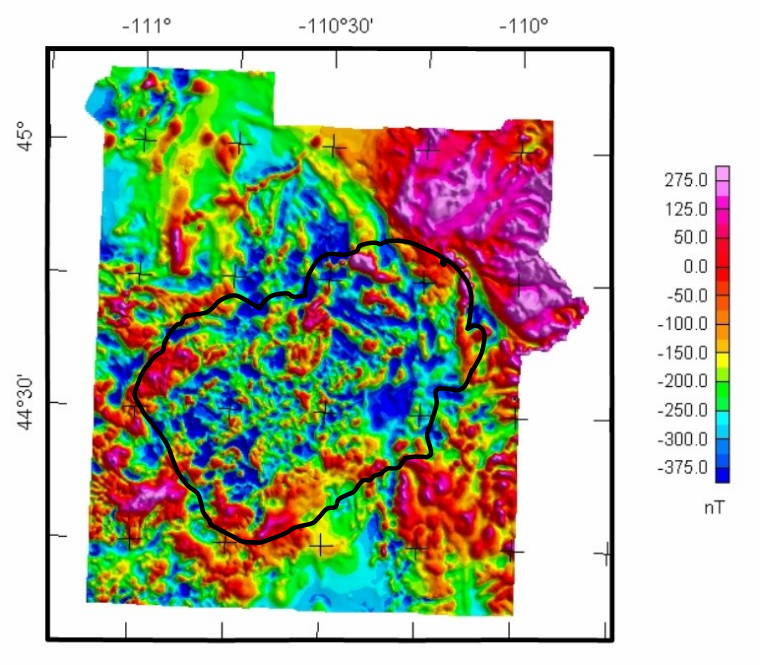

Figure 5. Aeromagnetic map plotted over the topographic map from U.S. Geological Survey, 1997

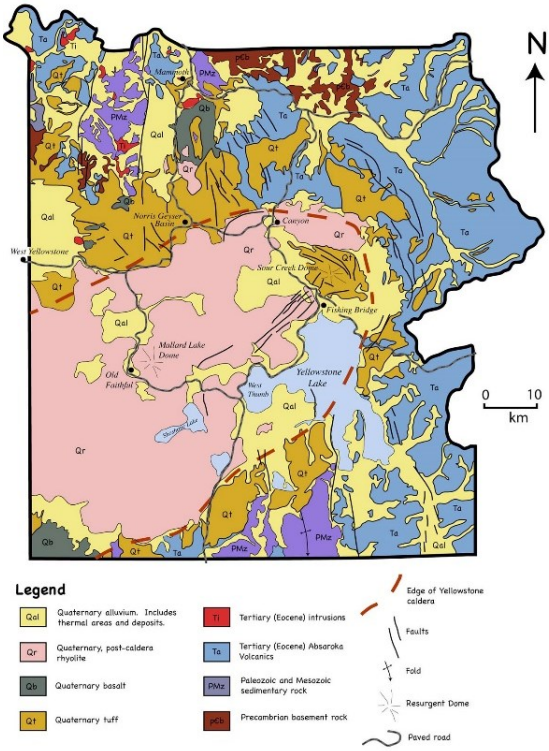

Figure 6. The Yellowstone National Park geological map modified from USGS I-711 by Miller, Oregon University

4.3. Methodology

I estimate the depth to the iso-Curie surface through two different spectral techniques: the centroid method and the fractal method. Both techniques are based on transforming the spatial total field data into frequency domain through a Fourier transform (Blakely, 1997), thanks to the relationship between the spectrum of the magnetic data and the depth of the magnetic sources (Shuey et al., 1977).

4.3.1. The estimation of the depth to the top and to the centroid from the power spectrum of magnetic field (modified centroid method)

Bhattacharyya (1966) presented the Fourier domain response of a rectangular prism. Later, Spector and Grant (1970), assuming a statistical ensemble of rectangular prisms, found the relationship between the slope of the logarithm of the power spectrum and the statistical average of the depth to the top of the source. In particular, they assumed a vertical-sided parallelepipeds, characterized by a joint uniform frequency distribution for the depth, width, length, depth extent, magnetization, and direction cosines of the magnetization (L, M, N) and the geomagnetic field vector(l, m, n).

$$P_s(\rho,\theta) = \left(\frac{u_0}{2}\right)^2 q^2 e^{-2h\rho}(1 - e^{-t\rho})S^2(\rho,\theta)R_T^2(\theta)R_k^2(\theta) \quad (4.1)$$

Equation (4.1) represents the spectral expression for a single parallelepiped (Bhattacharyya, 1966) in the polar coordinates, θ , where

$$S(\rho,\theta) = \frac{\sin(a\,\rho\,cos\theta)}{a\rho\,cos\theta}\,\frac{\sin(b\rho\sin\theta)}{b\,\rho\sin\theta} \quad (4.2)$$

$$R_T^2(\theta) = n^2 + (l\cos\theta + m\sin\theta)^2 \quad (4.3)$$

$$R_k^2(\theta) = N^2 + (L\cos\theta + M\sin\theta)^2 \quad (4.4)$$

$2a, 2b$ and t are the body dimensions, u_0 is the permeability of the free space ($4\pi \times 10^{-7}$ SI) and $q/4ab$ is the magnetic moment/unit volume of the body.

Spector and Grant (1970) used a statistical mechanics hypothesise that the mathematical expectation of an ensemble power density function was equal to an ensemble average. They assumed that all ensemble parameters were uniformly and independently distributed. The ensemble power spectrum could then be written:

$$P_s = \left(\frac{u_0}{2}\right)^2 \bar{q}^2\, C(\rho, \bar{a}, \bar{b})\, T(\rho, \bar{t})\, H(\rho, \bar{h}) \qquad (4.5)$$

$\bar{h}, \bar{a}, \bar{b}, \bar{t}, \bar{q}$, refer to the average parameter values of the ensemble. C is the azimuthal average, which deals with the range of the shape factor of an allowed widths and lengths (see Fedi et al., 1997); H is strictly related to the depth factor $\langle(e^{-2\bar{h}\rho})\rangle$ for depth variation $\Delta h < 0.5\bar{h}$.

Fedi et al (1997) and Quarta et al. (2000), recognized that the shape factor S in the Spector & Grant (1970) equation has a power-law form, for relatively large source horizontal dimensions,

$$S(k) = Lk^{-\beta} \qquad (4.6)$$

Where S is the shape factor of the power spectrum; L is a constant; k is the wavenumber and β is the sloping exponent, of the power-law: $\beta = 2.9$. The value of the scaling exponent represents the degree of correlation.

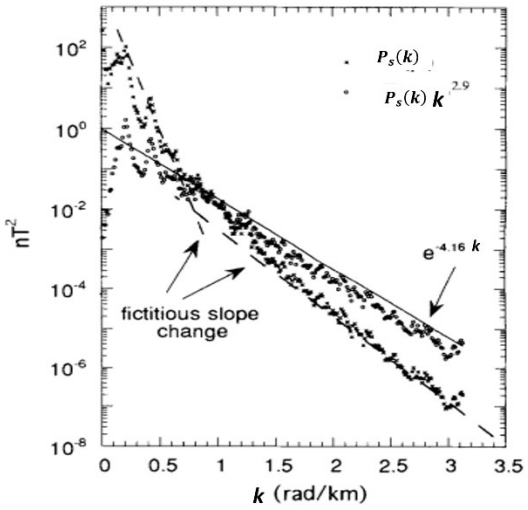

Figure 7. The correction technique for an ensemble of sources: the correction removes the fictitious deep slope change of the uncorrected spectrum (After Fedi et al., 1997)

According to Fedi et al (1997), the rate of decay of the power spectrum for a field at a h distance to the source top, is determined by two parameters: the exponent of the power law $-\beta$ and the exponent of an exponential-law factor, $2h$;

$$P_s \cong \left(\frac{u_2}{2}\right)^2 \bar{q}^2\, k^{-2.9}\, H(\rho, \bar{h}) \qquad (4.7)$$

So, to make an accurate estimate of the depth to the source, a power-law correction for the shape factor (approximately $k^{2.9}$) is necessary (Figure 7). For small sizes of the sources with respect to the data step (Fedi et al., 1997; Quarta et al., 2000), however, the correction has not to be applied, since the shape factor S tends to assume a flat shape (Figure 1, Fedi et al., 1997). So,

the power law correction is most suitable when the main behaviour of the anomaly field is characterized by rather extended anomalies.

For a horizontal layer with top at depth d and thickness t (Blakely, 1995), the power spectrum P_s can be written as:

$$P_s(k_x, k_y) = 4\pi^2 A\, P_{sm}(k_x, k_y)|\Theta_m|^2|\Theta_f|^2 e^{-2|k|Z_t}\left(1 - e^{-|k|(\Delta z)}\right)^2 \quad (4.8)$$

where k_x, k_y are wavenumbers in x and y directions, A is a constant, P_{sm} is the power spectrum of the magnetization; Θ_m and Θ_f are the directional factors related to magnetization and geomagnetic field respectively , Z_t, here is the depth to the top of the isothermal Curie depth and Δz is the thickness.

When this equation is used, usually the 2D power spectrum is transformed to a radial spectrum, which implies that the directional factors related to magnetization and geomagnetic field become constant. In case of a random and uncorrelated distribution of the sources, which means that we have a white noise distribution, the power spectrum of magnetization P_{sm} becomes constant as well.

Then, Equation 4.8 can be written as

$$P_s(k) = Be^{-2|k|Z_t}\left(1 - e^{-|k|\Delta z}\right)^2 \quad (4.9)$$

Where B is a constant and for a very thick magnetic body, the right-hand side of Equation 2 will contain only the depth to the top of the magnetized layer and it will be reduced as

$$P_s(k) = Be^{-|k|Z_t} \quad (4.10)$$

Equation 4.10 may be used to find the depth to the top.

Now, to find the depth to the centroid of magnetic layer, Bhattacharyya and Leu (1975) and Okubo et al (1985) applied the natural logarithm to both sides of the equation and later normalizing with the wavenumber

$$\ln\left(\frac{P_s(k)^{1/2}}{k}\right) = D - |k|Z_0 \quad (4.11)$$

Where D is a constant and Z_0 represents the depth to the centroid.

The depth to the bottom or the Depth to the iso-Curie surface is then computed as follow

$$Z_B = 2Z_0 - Z_t \quad (4.12)$$

Ōkubo et al. (1985) studied the Curie depth of Kyushu, Japan and suggested that centroid estimations could be derived from data windows what are as small as 40 km × 40 km, which however, can sometimes lead to estimate shallow (and maybe intermediate) layers but not deep ones. Tanaka et al (1999), assumed that the layer extends infinitely far in all horizontal directions, then the depth to the top of the layer is small compared to the horizontal scale of magnetic source. The magnetization in this case is also distributed in two dimensions (x and y). Moreover, for wavelengths less than about twice the thickness of the layer they were able to estimate the depth to the top by the slope of the power spectrum of the total field.

Equation 4.9 becomes

$$\ln[P_s(|k|)^{1/2}] = \ln M - |k|Z_t \quad (4.13)$$

Where M is a constant.

In order to estimate the depth to the centroid they rewrote Equation 4.2 as

$$P_s(|k|)^{1/2} = Fe^{-|k|Z_0}(e^{-|k|(Z_t-Z_0)} - e^{-|k|(Z_B-Z_0)}) \quad (4.14)$$

Where F is a constant. At long wavelengths, Equation 4.14 becomes

$$\ln[P_s(|k|)^{1/2}] = Fe^{-|k|Z_0}\left(e^{-|k|(-\Delta z/2)} - e^{-|k|(\Delta z/2)}\right) \sim Fe^{-|k|Z_0} 2|k| \frac{\Delta z}{2} \quad (4.15)$$

We can write then,

$$\ln\{[P_s(|k|)^{1/2}]/|k|\} = \ln M_1 - |k|Z_0 \quad (4.16)$$

Where M_1 is a constant.

The estimation of the depth to the top and the depth to the centroid can be done by fitting a straight line through the high-wavenumber and the low-wavenumber parts of the radially averaged spectrum of Equation 4.13 and Equation 4.16, respectively. In other words, from $\ln[P_s(|k|)^{1/2}]$ and $\ln\{[P_s(|k|)^{1/2}]/|k|\}$.

This method has been extensively employed to estimate the depth of the Curie surface (e.g. Bhattacharyya and Leu 1975; Okubo et al., 1985; Tselentis 1991; Tanaka et al., 1999; Dolmaz et al., 2005; Karastathis et al. 2010; Salah et al., 2013; Eletta and Udensi., 2012; Obande et al., 2014).

Although the centroid method is one of the simplest method to estimate the depth of the magnetic sources, it provides an overestimation of the depth values, the assumption of a random and uncorrelated distribution of sources (e.g. Pilkington and Todoechuck, 1993; Maus and Dimri 1994, 1996; Bansal and Dimri 1999).

Considering not a layer, but a statistical ensemble of prisms (Spector and Grant's model, Equation (5)) Fedi et al., (1997), showed how to correct for this overestimation by removing the shape factor.

4.3.2. The fractal Method

The fractal-based method for depth estimation has a similar approach, excepted for the scaling exponent, assumed constant (around 3) in Fedi et al (1997), while in the fractal method (e.g. Maus et al., 1997) is assumed a value within an interval of sloping exponents characterizing the fractal sources.

The method developed by Maus et al (1997) simultaneously estimated the fractal scaling exponents, depth to the top and the thickness of the magnetized layer.

$$P_s(k) = A - 2kZ_t - \Delta zk - \beta \ln(k) + ln\left[\int_0^{\infty}[\cos h\,(\Delta zk) - \cos(\Delta zw)]\left(1 + \frac{w^2}{k^2}\right)^{-1-\beta/2} dw\right] \quad (4.17)$$

Where β is the sloping exponent, controlled the source distribution, and w is the wavenumber in a vertical plane.

Bouligand et al (2009) were able to resolve all the integrals in Equation 4.11, which made it possible to be used and applied (see Bouligand et al (2009)).

In their tests on the synthetic data, Bouligand et al (2009) had difficulties estimating the depth to the top simultaneously with the scaling factor β and the thickness due to the uncertainties on the power spectrum. This is why they needed to fix the scale exponent from the beginning.

4.3.3. Limitations

Every method has its own limitations, but since the fractal analysis method and the modified centroid method belong both to the spectral methods, they do share some similarities and even most of the major limitations. The results of both methods are highly affected by the resolution of the used dataset (Comparing Figure 4 / Bhattacharyya (1975) and Figure 13 (my results)).

The obtained map of depths to the iso-Curie surface does not always represent the bottom of the magnetized crust, it can simply represent a lithological contact, a bottom of very high-magnetization sources (e.g. even a bottom of volcanic rocks).

Moreover, assuming that the measured magnetization is only horizontally distributed, can be not realistic.

Figure (8) represents the log spectra of the Yellowstone National Park magnetic data (Bouligand et al., 2009 and Fedi et al., 1997). The shape of the spectra predicted by the two models are almost identical. I used a power-law exponent of 2.9 for the fractal method. The spectra were performed using different thicknesses (0.1 km; 1 km; 2 km; 5 km; 20 km; 90 km and the infinity) in a very precise wavenumber range (from 10^{-7} rad/m to 10^{-1} rad/m).

The window choice is affected by the size of the map and the spacing used to do the grid (Nyquist - max). It is obvious, through the different windows used, that not all the windows can cover all the spectrum, except the window of 200 km going beyond the data area so it is not possible to use it. In the next sections I used some window sets that are ranging from 30 km to 50 km and then later I choose which one is the adequate for our case of study. For the modified centroid method, I used two set of windows: 30 km and 150 km.

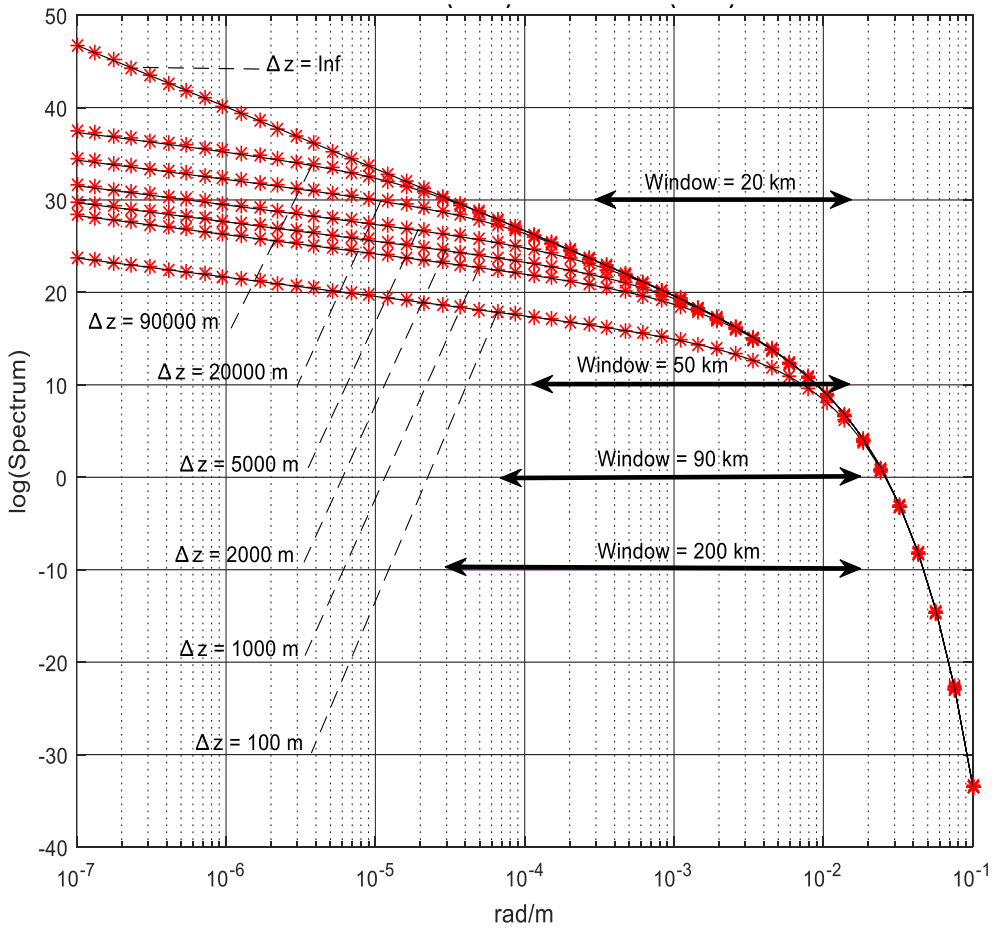

Figure 8. Log spectra vs the wavenumber [rad/m]: the red asterisk represents the spectrum after (Bouligand et al., 2009); and the black line represents the spectrum generated after Fedi et al. (1997)

4.4. Results and discussions

4.4.1. Modified centroid method

As mentioned in the in the methodology section, the basic 2-D spectral analysis method was described by Spector and Grant (1970). They estimated the depth to the top of magnetized rectangular prisms (DT) from the slope of the log power spectrum. Bhattacharyya and Leu (1975, 1977) further calculated the depth to the centroid of the magnetic source bodies. Okubo et al. (1985) developed the method to estimate the bottom depth of the magnetic bodies (DB) using the spectral analysis method of Spector and Grant (1970). Fedi et al (1997) corrected the Spector and Grant (1970) spectrum by a power-law of exponent 3.

Figure (9) represents the computed depth to the top (Figure 9.a) and depth to the bottom (Figure 9.b) of the magnetized layer. The window used to compute these result is 30 km and both maps are corrected using the altitude file grid provided by USGS (USGS, 2000). Both the black lines in the maps represent the limits of Yellowstone caldera: in Figure (9.a), the resulted depths are ranging from 0.8 km to 0.4 km. The shallowest depths (from 0.5 km to 0.4 km) are concentrated in the caldera area, whereas, for figure (9.b) the depths to the bottom or to the iso-Curie surface are ranging from 6 km to almost 1 km (the depths to the top DT are the shallowest and are concentrated in the caldera region).

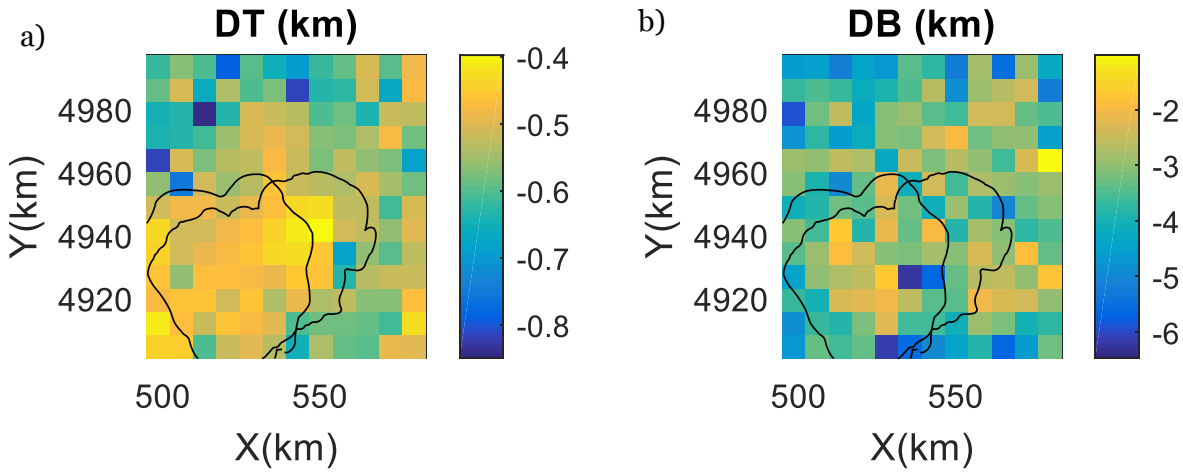

Figure 9. Depth to the iso-Curie surface (DB) and depth to the top (DT) of the magnetized layer from the modified centroid method using a 30 km window

Figure (10) represents the computed depth to the top (Figure 10.a) and depth to the bottom (Figure 10.b) of the magnetized layer, the window used to compute these result is 150 km. Both maps are corrected using the altitude file provided by USGS (USGS, 2000) and the black lines in the maps represent the limits of Yellowstone caldera. For figure (10.a), the resulted depths are ranging from 0.7 km to 0.45 km, the shallowest depths (from 0.5 km to 0.4 km) are concentrated in the caldera area. Whereas, for figure (10.b) the depths to the bottom or to the Iso-Curie surface are ranging from almost 6 km of depth to almost 1.5 km (the depths to the top DT are the shallowest and are concentrated in the caldera region).

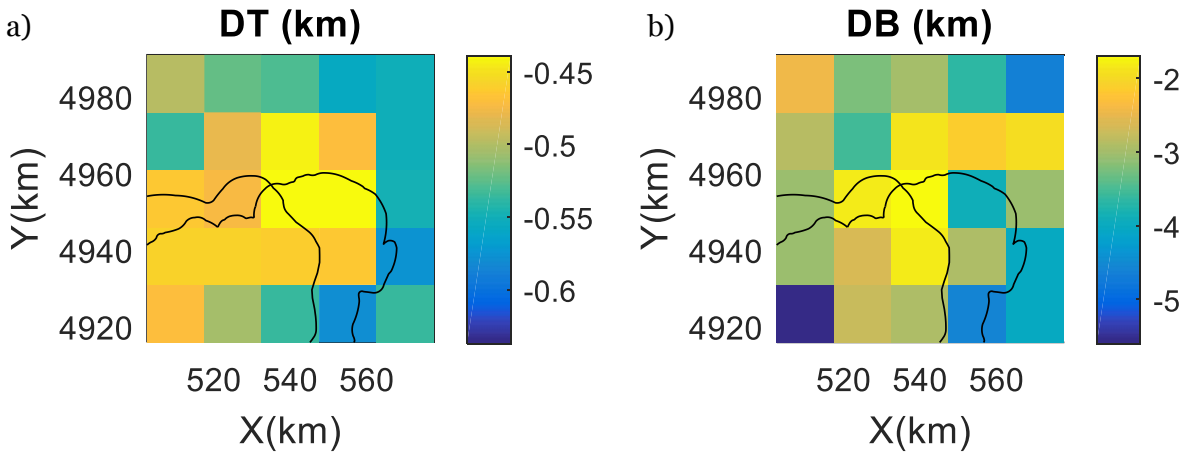

Figure 10. Depth to the Iso-Curie surface (DB) and depth to the top (DT) of the magnetized layer from the modified centroid method using a 150 km window

4.4.2. Fractal analysis method

As mentioned in the methodology, the fractal analysis of magnetic anomalies were first introduced by Maus et al. (1997), and then developed by Bouligand et al., (2009): it belongs to spectral analysis, where the power spectrum of time series is plotted against frequency (or wave number in the case of space series) and the value of slope, known as scaling exponent (mentioned before as beta or β), controls the balance of high and low frequencies and determines the degree of correlation of the series.

Since the best result of the fractal analysis method is based upon the best choice of the scaling exponent and of the swiping window, I performed several tests (Figure 11 and Figure 12) in order to choose, the best scaling exponent range and the best window range. The choice is based on the root mean square error: wherever it's the lowest, I use the corresponding parameters.

All the results in Figure 11 were reached using scaling exponent of 3. The choice to present the results of the scaling exponent ($\beta = 3$)was made not only after taking into account the result of the study of Bouligand et al (2009) but also because I used all different betas and the best and the acceptable ones are around 3 (see Figure 11). The figure itself includes three graphs, where c) graph represents the Root Mean Square (RMS) of an iteration on a set of windows that are going from 20 km to 90 km. In other words, I was applying the fractal analysis method on the aeromagnetic data using each time a window that start from 20km to 90 km, every 0.5 km. The b) graph represents the corresponding thickness of each window. Figure 12a shows the depth to the top (DT) versus the windows interval.

The smallest RMS is concentrated from window of about 25 km to a window of almost 50 km, which give us the information that the expected DT and thickness are going to be respectively shallow and thin.

The expected DT are going to be ranging from 0.270 km to 0.350 km and the thickness is expected to be ranging around 3 km to 4 km.

One last and important thing to mention, analyzing Figure (11), is that the results are largely dependent on the window size, which itself confirms the results assumed describing Figure (8).

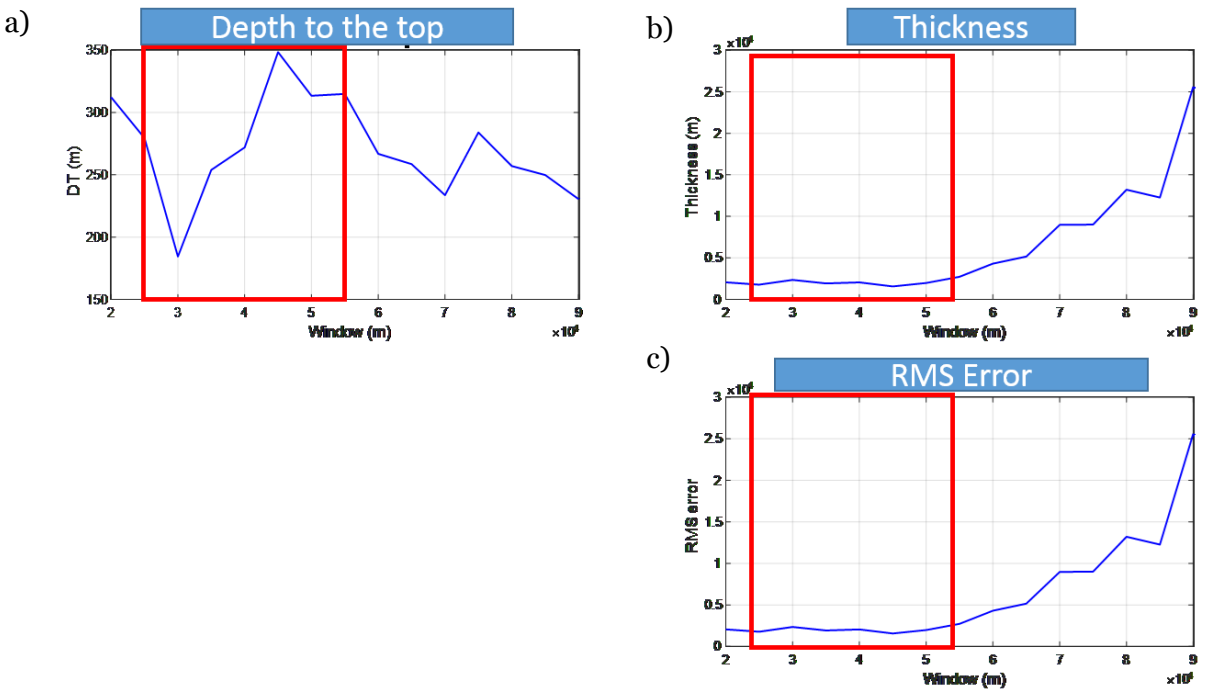

Figure 11. Testing the best range of windows (from 20 km to 90 km)

The results shown in the graphs of Figure 12, were calculated using a window size of 30 km. As in Figure (11), c) graph, represents the Root Mean Square (RMS) of an iteration realized on a set of sloping exponents that are going from 2 to 4. In other words, I was applying the fractal analysis method on the aeromagnetic data using each time a different scaling exponent number ranging from 2 to 4 and with a step of 0.1. The Figure 12b graph represents the corresponding thickness of each scaling exponent. Figure 12a shows the depth to the top (DT) versus the sloping exponent interval.

The shallowest RMS is ranging from the scaling exponent of 3 to the scaling exponent of 3.6, which align with the previous result of windows: It is expected a DT and thickness respectively shallow and thin.

The expected DT in this case are going to be ranging from 0.2 km to 0.15 km and the thickness is expected to be ranging around 2 km to 1.5 km.

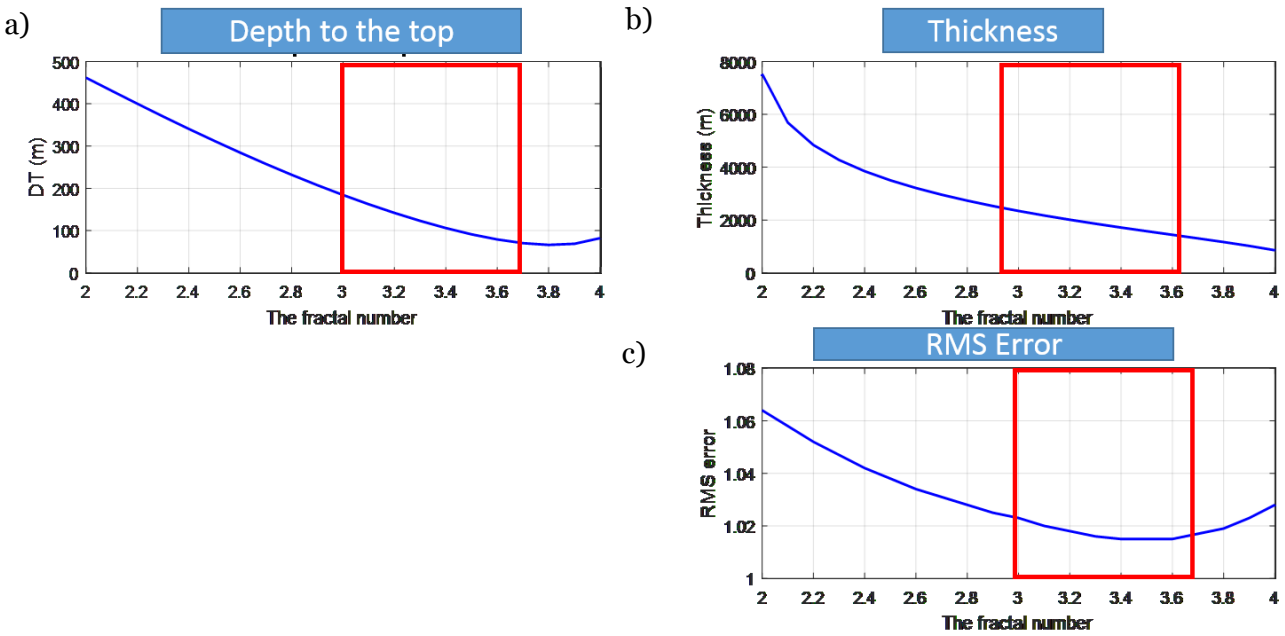

Figure 12.Test the best ranging of the scaling exponent.

Like the window size and the scaling exponent tests, I performed different tests trying to choose the best wavenumber limits applied to our study.

For each scaling exponent, I applied the fractal analysis method and I obtained a different result using all the window sizes that are adequate (Figure 11).

Concerning the main result of the fractal analysis in investigating the depth to the Iso-Curie surface at Yellowstone, Figure (13) represents the obtained final result:

- DT represents the depth to the top of the magnetized layer: this map is corrected using the altitude file provided by (USGS, 2000). The depths are ranging from 0.25 km to 0.05 km slightly above the sea level. The shallowest depths to the top are concentrated in the Caldera area. The peripheral areas have the deepest depths (deeper than 0.300 km).

It's important to mention that the depth to the top map was consistent during all the tests. The shape of the depth anomaly has never change.

- DB represents the depth to the bottom of the magnetized layer, which I consider as the Curie isotherm or the depth to the Iso-Curie surface. The depths are ranging in the map from 1 km to 5 km; the shallowest depths are concentrated in the caldera area as for the depth to the top; depths outside the caldera can reach more than 5 km.
- Normalized RMS represents the normalized root mean square (NRMS). The map shows NRMS ranging from 0 to 2 with 1 represents the best results. The overall NRMS values in the map are ranging from 1 to more than 1.5 outside the caldera.

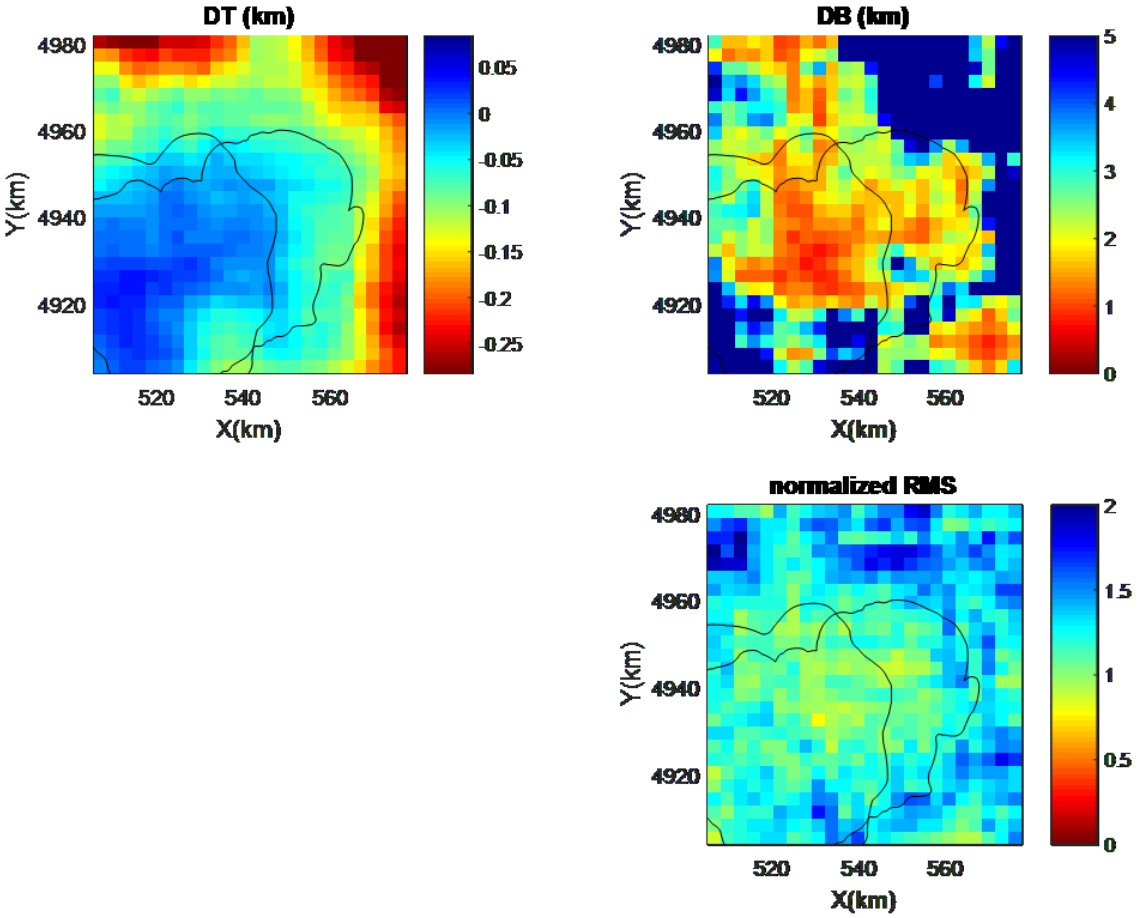

Figure 13. The best result of the fractal analysis method.

To certain the obtained results, I opted to pre-set the depth to the bottom acquired from our final result (Figure 13) and applying the fractal method another time to double check the consistence. In other words, the acquired result state that the depth to the bottom of the magnetized layer inside the caldera is around 1 km, then I set the depth to the bottom to that value everywhere in the map in order to check the result of the NRMS. The result was satisfying (Figure 14), since everywhere in the map has a very high error except inside the caldera area where I have a Normalized RMS of 1 which means that the model-generated data and the measured data are so close.

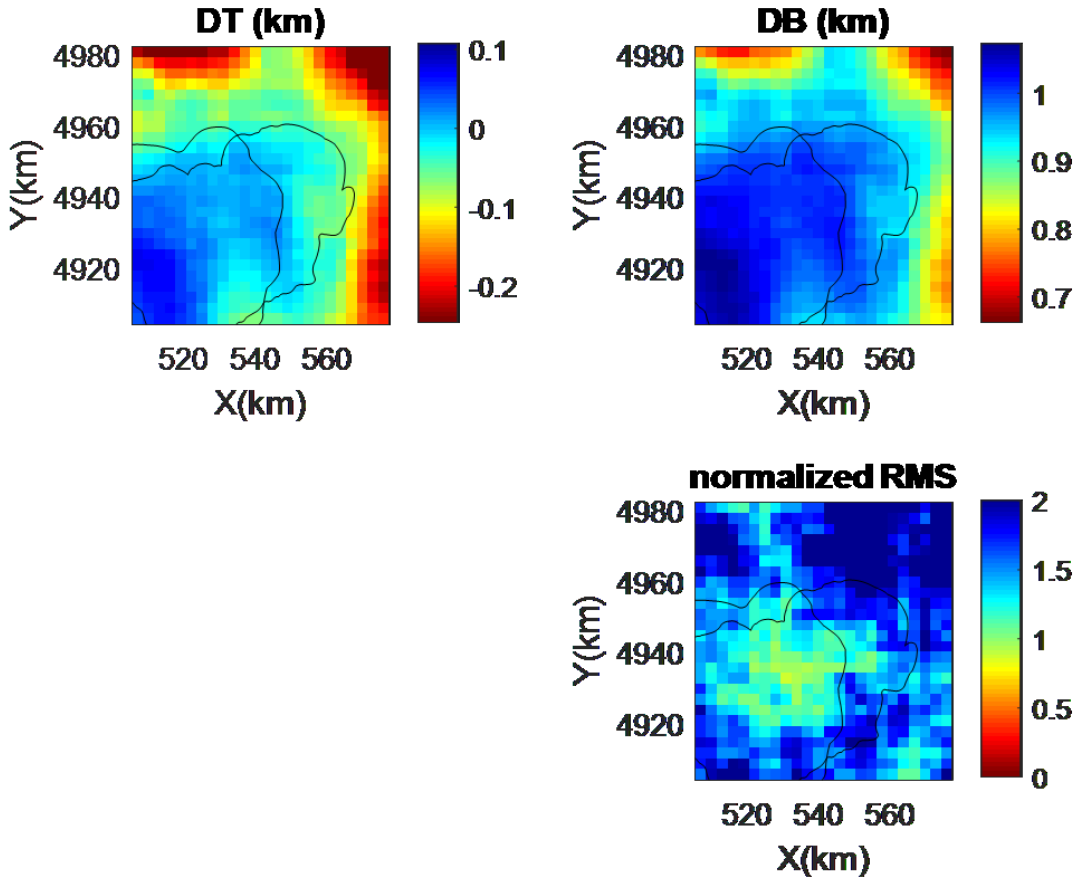

Figure 14. Checking the Validity of our results inside the caldera

The Depth to the top (DT) in Figure (14), conserved the same feature shape of the original depth to the top map. It is relatively deep outside the caldera and shallow inside it.

Now, in order to check the depths outside the caldera, I assumed a depth to the bottom of the magnetized layer of 5 km (Figure 15). I remark that the normalized Root Mean Square is acceptable outside the caldera but not inside of it. This result demonstrates that assuming 5 km as a depth to the bottom can be acceptable, which means also that all retrieved depths outside the caldera that are around that value are acceptable too.

To sum up the result of the fractal analysis method, I retrieved a depth to the Iso-Curie surface that is ranging from 1 km inside the caldera to 5 km outside the caldera. This shallow depths are so how expected since we have a very hot zone with a very high heat flow (Smith et al., 2009).

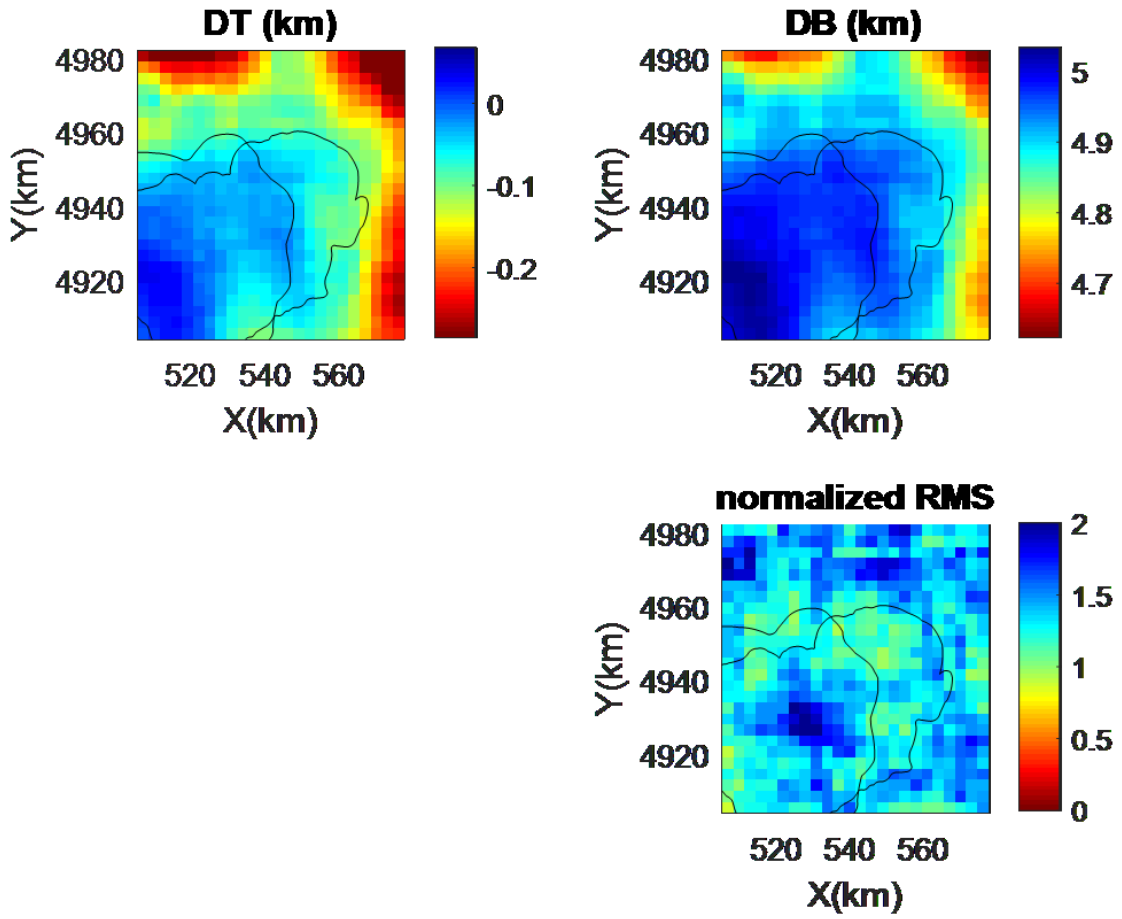

Figure 15. Checking the Validity of our results outside the caldera

4.5. Conclusions

This Chapter summarize the work performed to investigate the depth to the isocurie surface under Yellowstone. It is made of a comparison between two techniques derived from the same family of method (Spectral analysis methods) but with different approach and different assumptions but basically the same limitations.

The best results acquired from the fractal analysis method is obtained with a law-power exponent equal to 3, which is equivalent to the correction applied by Fedi et al (1997) to the Spector and Grant (centroid method) (1970).

The results achieved from the fractal analysis and the modified centroid method show the same range of depths (from 1 km to 5 km), and relatively the same distributions. The shallowest depths are located inside the caldera and the deepest depths are located everywhere else.

The estimation of the most suitable fractal sloping exponent led to a value equal to the fixed sloping exponent of the corrected Spector and Grant method, which imply that the two methods have given basically the same result.

Using the depth to the Curie isothermal surface, we could obtain a heat flow estimation using the same parameters of Bouligand et al (2009) since they were used for western USA and they were acceptable.

The acquired depth to the isocurie map was used later as a very important constraint to check the validity of the 3D thermal model I am going to build and present in the next chapter (see chapter 5).

Chapter 5: 3D thermo-rheological model of the crust beneath Yellowstone caldera

5.1. Introduction

The geodynamic processes of the crust plays a key role in controlling the thermal structure of the Earth. Therefore, a good knowledge of thermal conditions is crucial for a quantitative understanding of a wide variety of geological processes and rheological/rock-physics parameters in general (e.g. Bansal et al., 2011).

A thermal area is a contiguous geologic unit generally including one or more thermal feature, bounded by the maximum areal extent of hydrothermally altered go round, hydrothermal mineral deposits, geothermal gas emissions, or heated ground (Jaworowski and others 2010).

The Yellowstone hotspot is a continental hotspot, responsible for the large scale volcanism in Oregon, Nevada, Idaho and Wyoming states (USA) where is located the Yellowstone National Park. On this context, the North American tectonic plate movements across the Yellowstone hotspot has formed the Eastern Snake River Plan through a succession of caldera-forming eruptions.

In this geodynamic scenario, the Yellowstone geothermal system is the surface manifestation of partly molten magma reservoir that exists beneath the 0.64 Ma Yellowstone Caldera (Christiansen, 2001) with over 10,000 geysers, hot springs, and fumaroles. It has the world's highest concentration of hydrothermal features reflecting its extraordinarily high convective ground water circulation (Fournier, 1989). The large hydrothermal systems are considered to be the result of hot water circulating along fractures in the crust heated by crystallizing magma (Fournier, 1989).

The active hydrothermal, magmatic, and tectonic system in Yellowstone can cause a future violent events and make it a highly potential hazards to the area.

Despite the huge amount of studies on Yellowstone caldera, a detailed analysis on determining the thermal-rheological state of the crust under this caldera has not yet been performed. This is for different reasons, among which the most important one, is the difficulty to measure and discriminate the nature of the heat flow for the active role played by the convective and conductive thermal regime.

In this context, assessing the Curie surface coupled with the conductive finite element thermal model, allow us to discretize the thermal distribution of the crust and to compute a 3D rheological model as well.

In this chapter I firstly analyse the crustal thermo-rheological state beneath Yellowstone, by performing a finite element temperature model using the existent data and then produce a 3D rheological model for defining the brittle ductile transition and finally a relationship between seismicity cutoff and rheological condition of the study area will be displaced.

5.2. Collected Data

In this section, I display the amount of the multiplatform from dataset employed in the realization of the crustal thermal model and the 3D rheological model.

One of the most important piece of data used in this part of the work is the Curie isotherm surface as results from Chapter.4 /Figure 13, which will be used as a temperature constraint to check the validity of our thermal model: in particular, I used the isocurie surface calculated using the fractal analysis method, like a constrained surface to evaluate the certainty of the model. Most data used in this chapter are taken from previous research (e.g. Smith et al., 2009; Farrell et al.2014; Husin et al., 2014; Huang et al., 2015).

I retrieved the density model (Figure 17) of the crust under Yellowstone using the tomography model (Figure 16) performed by Huang et al (2015) applying the Lindseth equation (Lindseth, 1979).

The present velocities are ranging from 3000 m/s on the surface where, the location of the magma chamber (from about 5 km to 8 km of depth) under the caldera limits (red dots in the figure), to 7500 m/s at the base of the model (from about 40 km to 44 km, the last depth of the model).

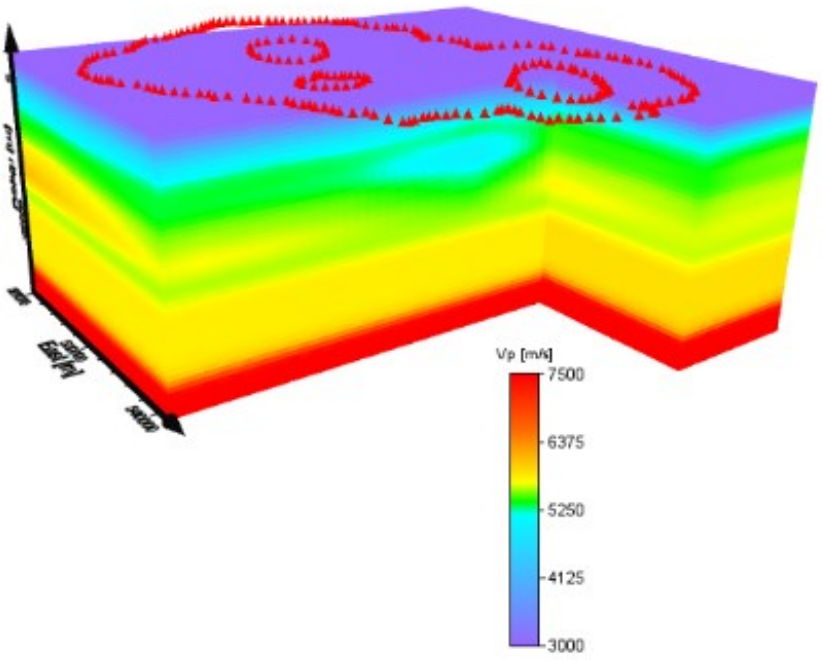

Figure 16 Tomography model after (Huang et al., 2015)

As mentioned before, the density model was performed, using the Lindseth (1979) relationship. Accordingly, the densities of the model (Figure 17) are ranging between 2600 kg/m^3, as expected by the presence of the magma chamber which is a rhyolitic magma, to 3000-3200 kg/m^3 at the base of the volume. I can notice variability of densities (from 2900 to 2950 kg/m^3) exist also inside the volume, attesting a heterogeneous density distribution into the model.

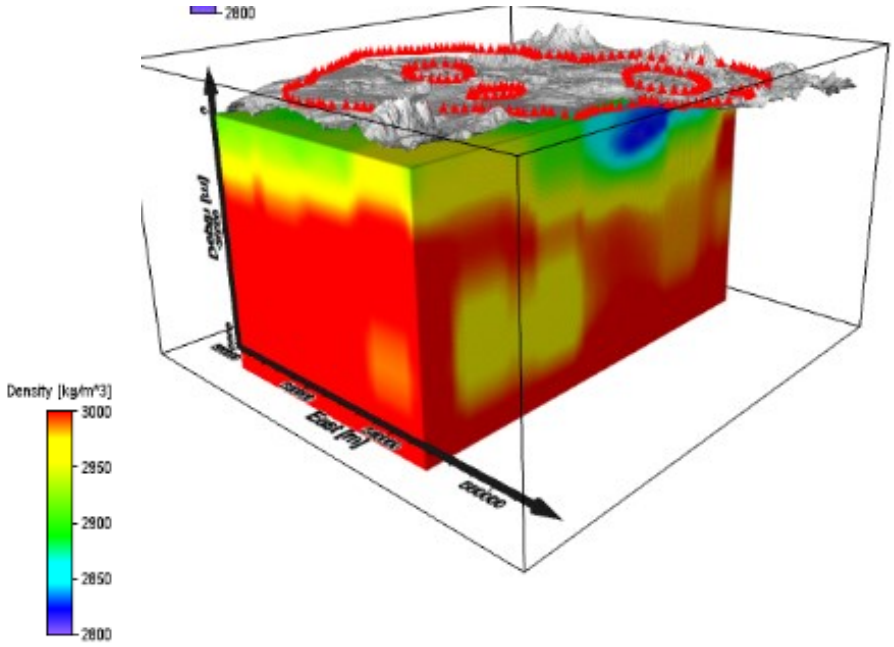

Figure 17. Density model after (Huang et al., 2015)

For the heat production source (Figure 19), I used the density model generated after Farrell et al (2014) and optimized later in the present study.

Other important data used in this study was the heat flow measurements (e.g. Smith at al., 2009; Blackwell et al., 2011). They were used to control the resulted heat flux on the surface.

Based on the priori available geophysical and geological information, I was able to generate a 3D finite element models using a Comsol Multiphysics environment: I performed a 3D Finite Element modeling of thermal field, by optimizing the heat production of the detected magma source in order to provide the best crustal temperature configuration that minimize the distance between the observed superficial heat flow and the performed iso-Curie surface.

Another important data to mention are the drillholes presented in that area (White et al, 1979), but since these wells are not deep enough to estimate the geothermal gradient, I chose the heat flow information measured at the surface.

5.3. 3D thermal Finite Element Model

Like many volcanoes, Yellowstone has an active hydrothermal (hot water and steam) and geothermal system that resides between the Earth's surface and the underlying magma.

According Castaldo et al. (2017), the physical heat regime considered is just conductive transfer, which means excluding the radiation and the convective. I carried out a 3D thermal finite element model of the first 44 km of the crust. The physical study as well was assumed to be time independent where all the field variables were considered constant and, the main temperature equation corresponds to the differential from Fourier's law that contains in our case an additional contribution which is the heat production generated from the source.

Therefore, the governing equations meant to be solved in this specific regime case (conductive) and under these assumptions are:

$$\rho \times C_P \times \nabla T = -\nabla \cdot \mathbf{q} + Q \qquad (5.1)$$

Where, ρ represents the density of the rocks in kg/m^3, C_P is the specific heat capacity measured in J/kg/K, T is the absolute temperature K, **q** is the conductive heat flux vector measured in W/m^2 and Q is the volumetric heat source production that is measured in W/m^3. The conductive heat flux vector is expressed by the next equation

$$\mathbf{q} = -k \times \nabla T \qquad (5.2)$$

Where k, is the thermal conductivity measured in W/m/K.

The computational domain is characterized by a size of $66900 \times 77300 \times 44000\, m^3$. The defined 3D mesh geometry (Figure 18) is controlled by 181553 tetrahedral elements characterized by 12 vertex elements, 543 edge elements, 15475 boundary elements and a maximum element size of 3000 m and a minimum of 300 m.

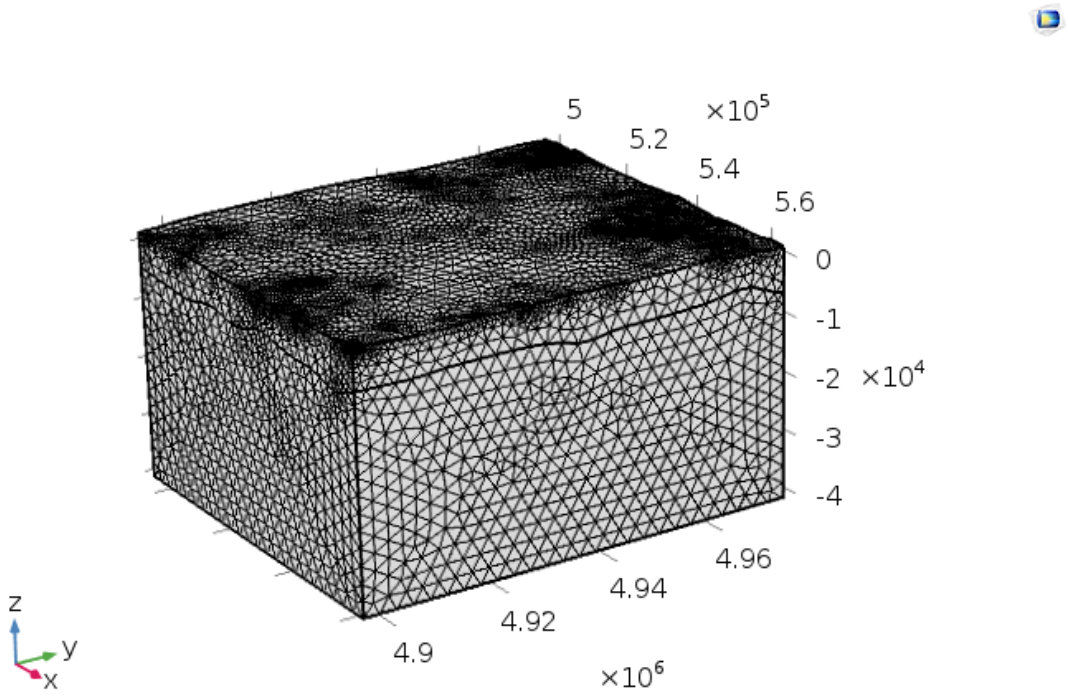

Figure 18. The finite element method meshed

The generated mesh is further validated through several resolution tests (Jiaxiang, 1998), which suggests that the use of a finer mesh would only improve the results of less than 5%.

A natural geothermal gradient (about 33 °C/km), has been used for the first 5 km, while another gradient has been implemented, as suggested from a quick study on the geothermal gradient in Yellowstone (White et al., 1975), as initial values of temperature.

I used the density from the available velocity tomography model (Huang et al., 2015) as mentioned before. Gardner et al (1974) have shown that density is closely proportional to the one-quarter power of velocity, the relation varying slightly with rock type. In our case in order to calculate the density, I am using the model from Lindseth (1979) where

$$V = 0.308\,\rho V + 1054 \qquad (5.3)$$

V represents the P velocity in m/s derived from Huang et al (2015), ρ is the density kg/m^3.

In this study, I tried to identify the source by extracting the density from the tomography performed by Farrell et al. (2014) and found a heat source corresponding to the magma chamber, as shown in Figure (19). Unlike several studies consider the magma chamber as a spheroid or the sum of two spheroidal sources (e.g. Battaglia et al, 2003, Tizzani et al., 2015; Vasco et al., 1990), I found that it rather appears as an oval shape.

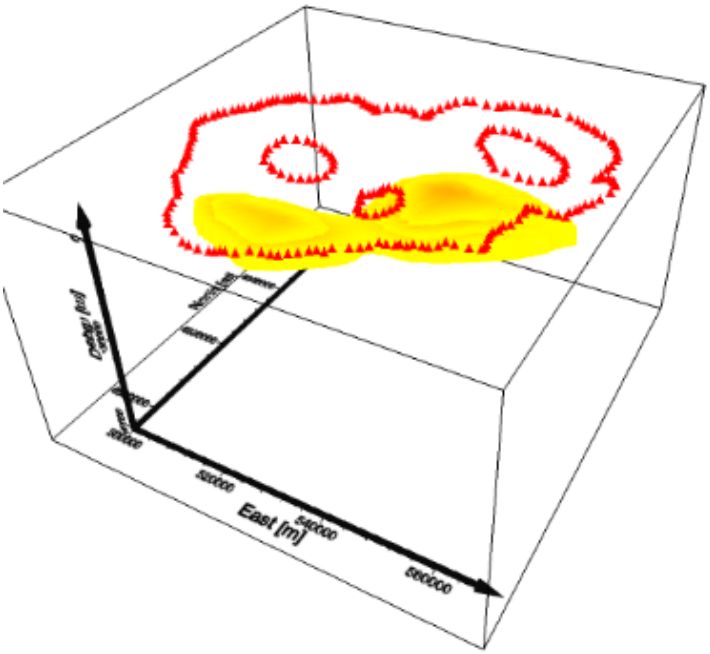

Figure 19. The considered heat source geometry after Huang et al. 2015

According to previous volcanological studies, basaltic lavas have erupted around the margins of the active, mainly rhyolitic Yellowstone Plateau volcanic field throughout its evolution. The absence of basalts from within the rhyolitic source areas is interpreted to reflect the trapping within the crust of any basaltic magma that might have intruded from zones of partial melting in the upper mantle beneath crustal rhyolitic magmas of lower density (Christiansen, 2001).

Only after about a million years have basalts erupted through the cooled, crystallized, and fractured upper-crustal magmatic sources of the first and second rhyolitic cycles, no basaltic vents, however, occur within the third-cycle Yellowstone caldera. A few small outcrops of basalt do occur on the northwest caldera wall near Purple Mountain (Christiansen and Blank, 1974), but they are erosional remnants of lavas that flowed down the steep slope from vents farther north. Additionally, some rare quenched inclusions of basaltic magma were found within the basal part of the rhyolitic West Yellowstone flow near the crest of the Madison Plateau west of Little Firehole Meadows (Christiansen and Lipman,1972), suggesting that basaltic magmas from lower-crustal levels might have played a role in mobilizing some intra-caldera rhyolitic magmas for eruption.

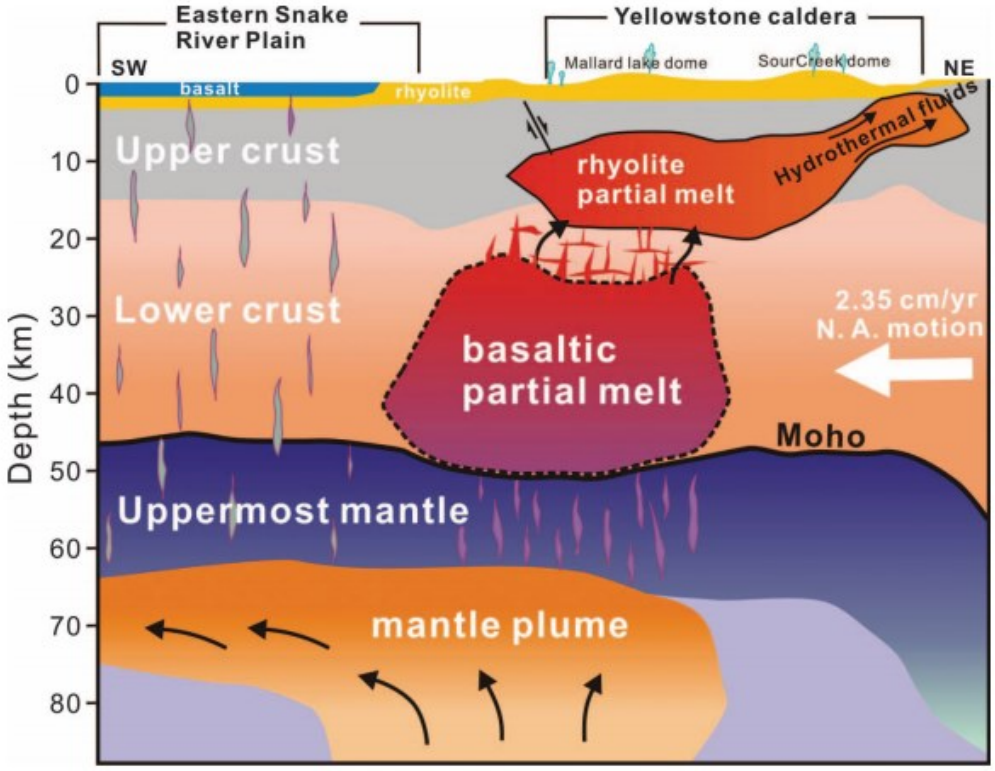

Figure 20. Schematic model for the Yellowstone crust–upper mantle magmatic system (e.g. Farrell et al, 2014; Huang et al., 2015).

Shen et al (2013) suggested that the Moho is situated at 45 km (Figure 20) which was also used by Farrell et al (2014) and then by Huang et al (2015), whereas Bouligand et al (2009) suggested that the Moho discontinuity is situated at about 40 km. I opted for the Moho depth of 44 km in our model.

In order to find the best-fit solution on Yellowstone caldera, I used a trial and error optimization of the geothermal heat production source and the parameters applied for generating the temperature model.

The boundary conditions were set in order to enhance and to give some real limitation to the finite element model: I considered an outgoing heat flow at the lower part of the computational domain, which represents the local Moho discontinuity, a temperature condition at four sides of the domain, assigned to the above mentioned geothermal gradient.

All the model parameters employed in the optimization are procedure are presented in Table (1).

Table 1. Parameters used to perform the model

density	2600-3200 [kg/m^3]
specific heat capacity	850 [J/kg/K]
thermal conductivity	1.5 [W/m/K]
volumetric heat source production	6.10^{-5} [W/m^3]

A very quick study was performed on the basis of the existent drillholes in Yellowstone national park (Figure 21), most of the drillholes are inside Yellowstone caldera, on the central plateau.

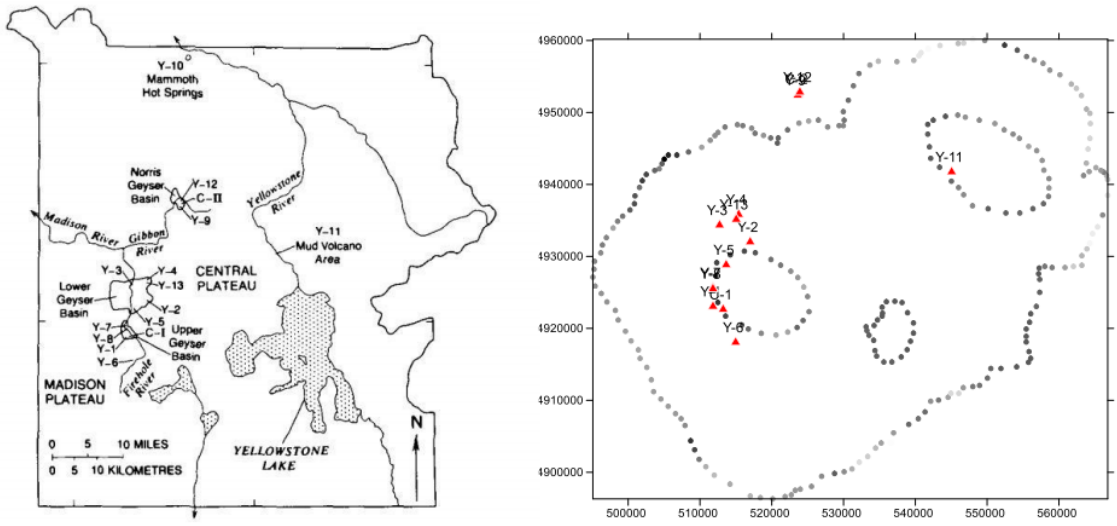

Figure 21. Position of the drillholes in the Yellowstone National park and in the caldera from (White, 1979)

The studied 15 wells are very shallow. Figure (22), shows a representation of depth versus temperature. It illustrates the fast trend of the temperature with the depth. Also, the maximum achieved depth is less than 0.2 m, which means that they are too shallow to be considered, thus they will be excluded in our modelling approach.

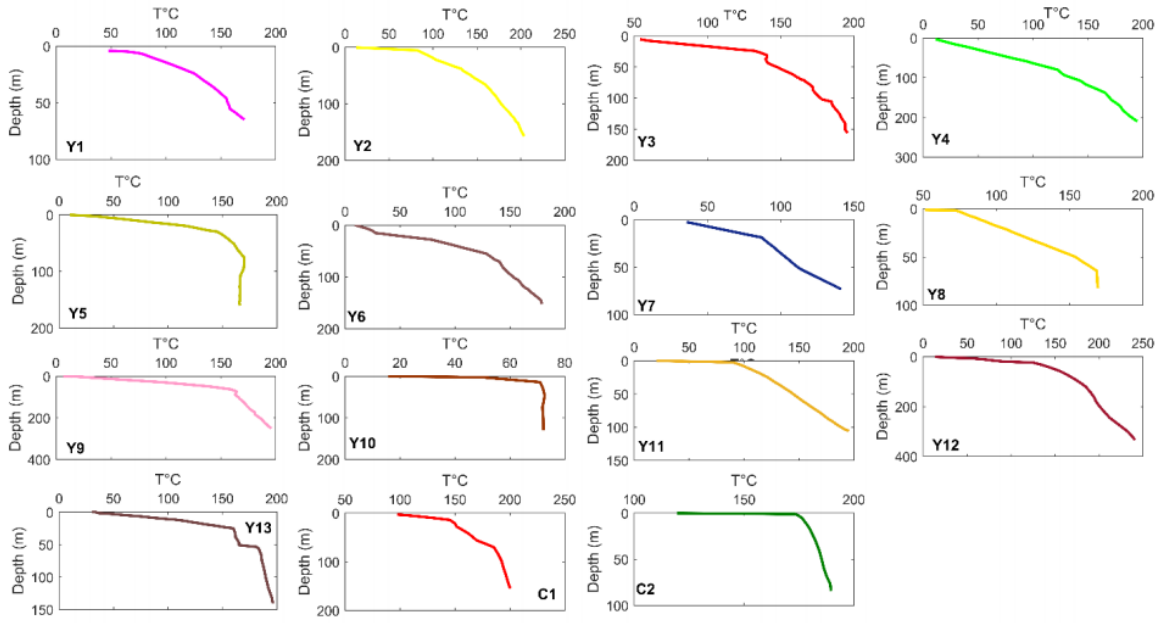

Figure 22. Depth vs temperature plots for the well collected after (White et al., 1975)

The retrieved thermal model is represented in Figure (23). It shows the temperature distribution beneath Yellowstone caldera. The result of the finite element conductive thermal model point out the existence of thermal anomaly region ranging from 55 °C (on the surface) to 1120 °C (at the base of the volume solution) which corresponds to a depth of about 40 km (Figure 23). These range of temperature is confirmed by different studies (e.g. Horwitz and Lowenstern, 2014/ Figure 5), where it is shown that the base of their model (deeper than 45 km unlike our case) is composed by a rising basaltic magma whose temperature is about 1200 °C and that the magmatic chamber is constituted of rhyolite whose temperature is about 800 °C.

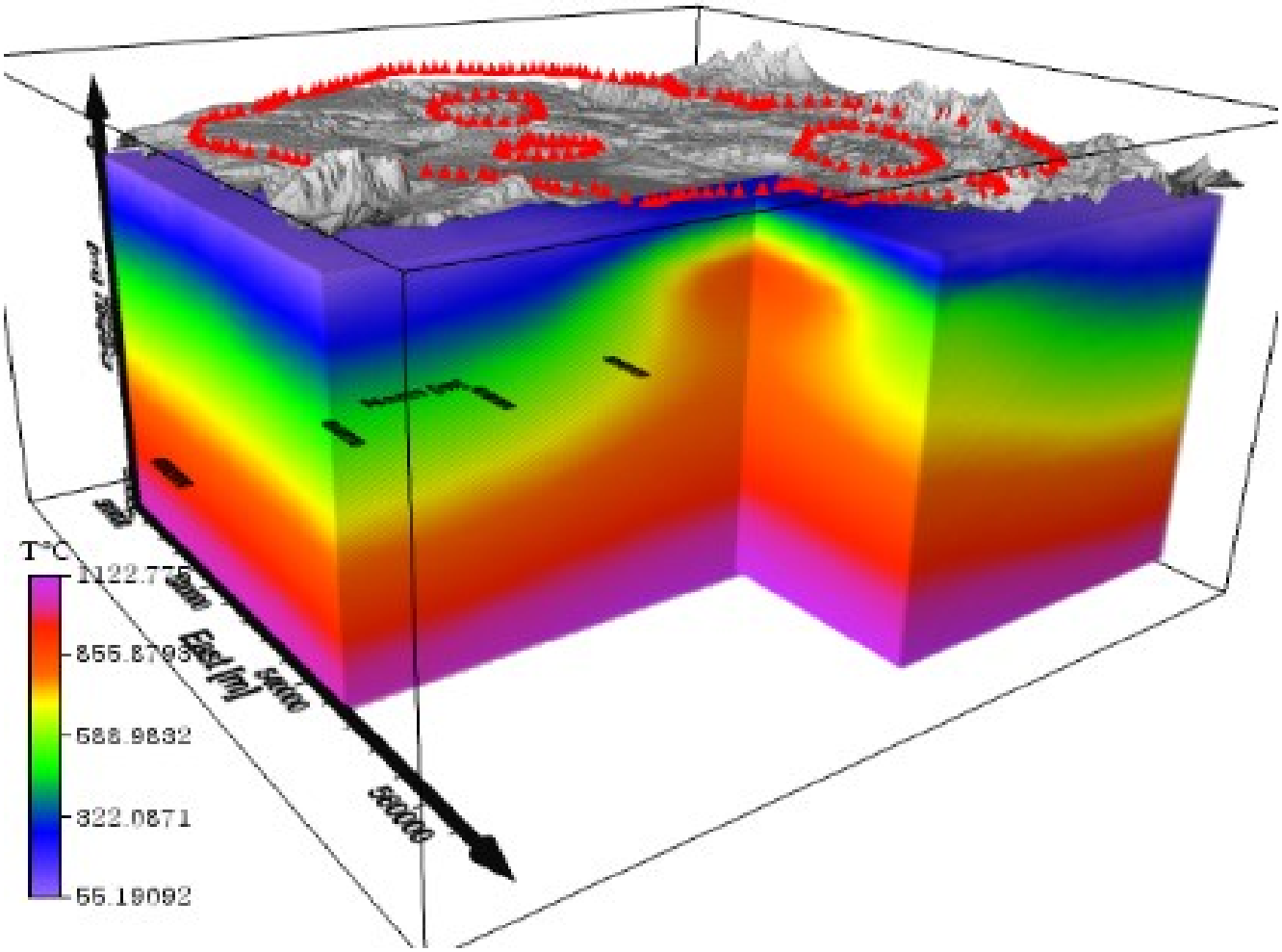

Figure 23. 3D thermal model of the crust under Yellowstone

To improve the retrieved temperature model, I compared the iso-Curie surface extracted from the thermal model and the iso-Curie surface already computed from the aeromagnetic data (see Chapter4).

Figure (24), represents the computed finite element thermal model with the extracted iso-Curie surface at 500 °C, this isotherm, which is represented by the orange surface (Figure 24) appears to be very shallow, above the magmatic chamber and deeper going to the edges of the crust.

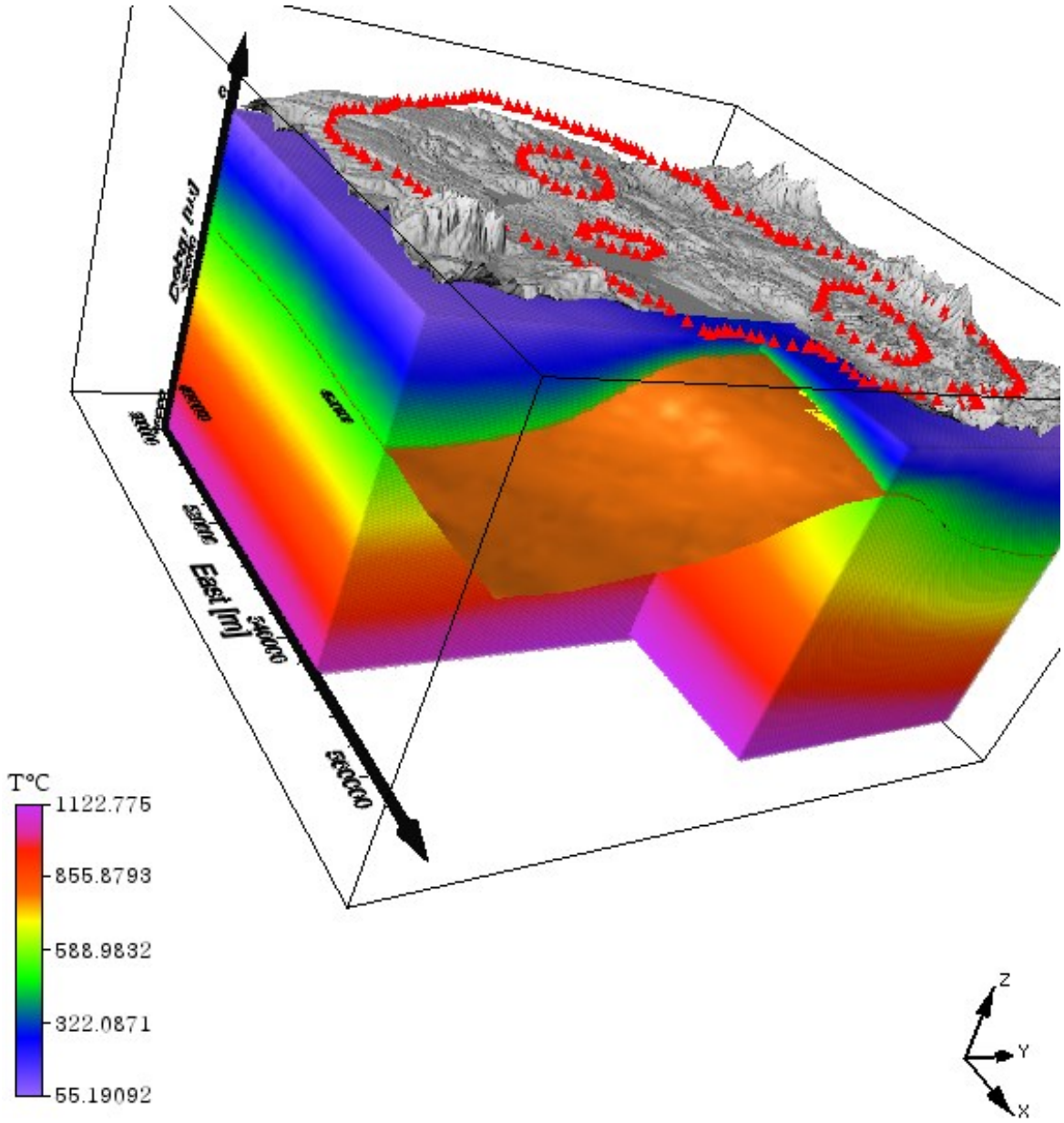

Figure 24. The thermal model with the extracted isocurie surface.

A comparison between the Curie surface obtained from the finite element model and the depth to the Iso-Curie surface obtained from the aeromagnetic data (Figure 25), shows that in the caldera area (blue square in the Figure 25) there is a low misfit (RMSE). In Figure (25), SA represents the depth to the Iso-Curie surface obtained from the spectral analysis methods (see

Chapter 4) while FEM, represents the Curie surface resulted from the finite element modeling (Figure 13). The RMSE is ranges from 1.8 in the SW-NE profile P1, to 2.4 in the NW-SE direction of the Profile P4.

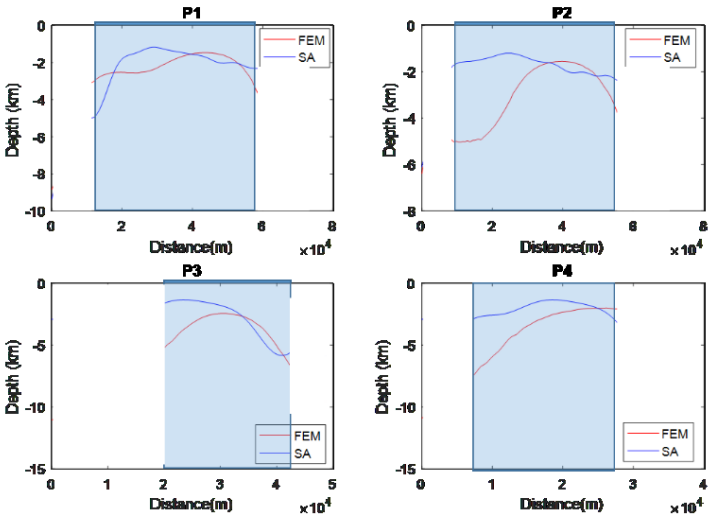

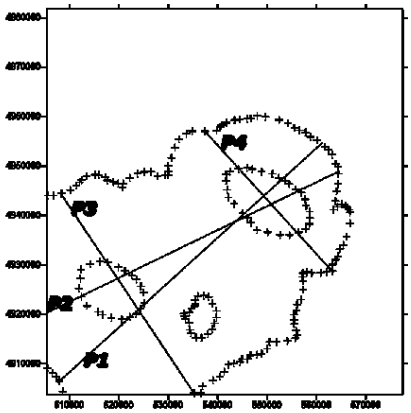

Profile	RMSE
P1	1.8
P2	2.07
P3	1.9
P4	2.3

Figure 25. Comparison between Depths to the curie surface obtained from the finite element modeling (FEM) and the fractal method of the spectral analysis (SA); RMSE means the root mean square error in the blue area which represent the caldera region.

A slice of the temperature model at 4500 m of depth is reported in Figure (26), it appears to perfectly fits perfectly the location of the source in the volume with a temperature ranging from 200 °C in the edges to a higher temperature at the magmatic chamber (higher than 700°C).

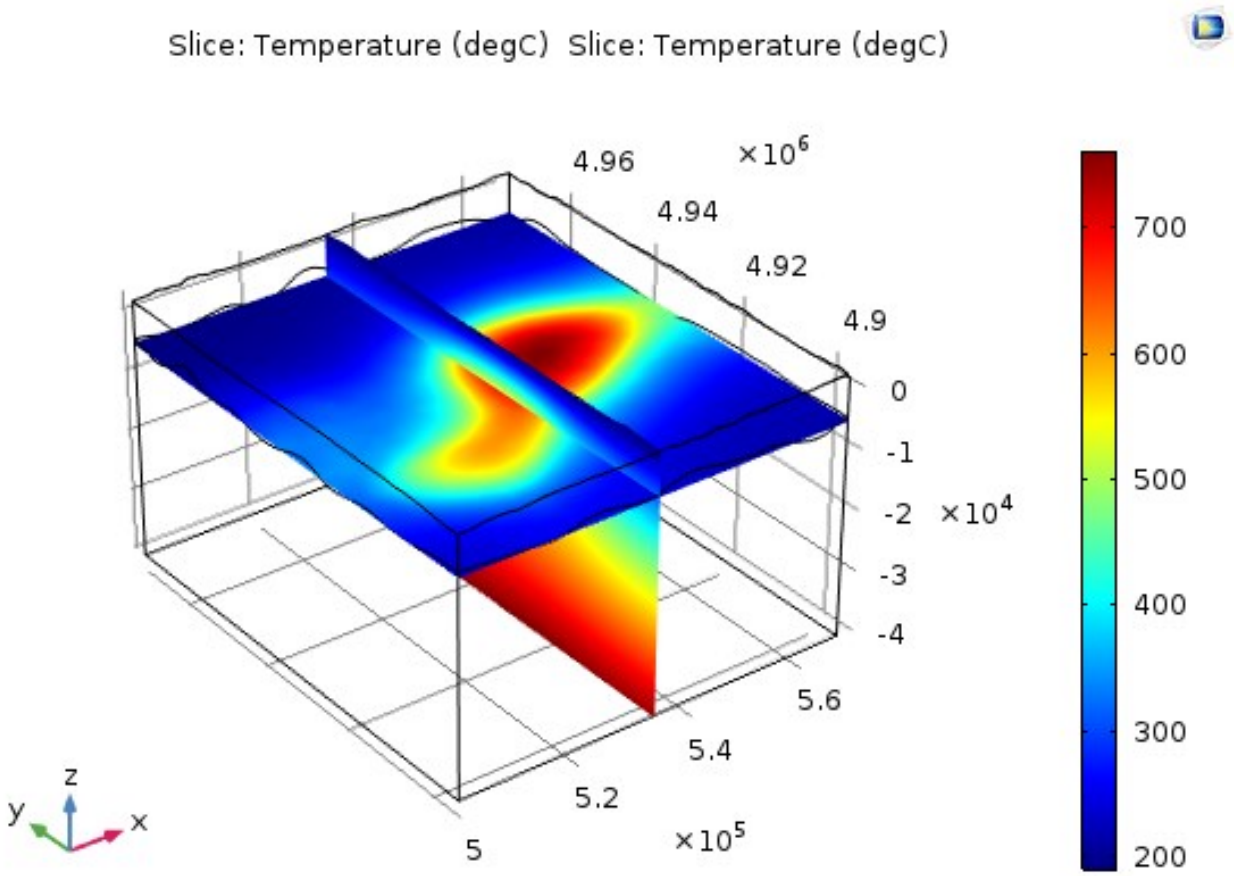

Figure 26. Temperature sliced at 4500 m of the volume.

I have also computed the volumetric heat flow. The Figure (27) reports the heat flow at the surface, where the conductive heat flux ranges from zero W/m² to 0.14 W/m² above the magmatic

source, confirming the study which has been done by Smith et al. (2009) and by Blackwell et al. (2011).

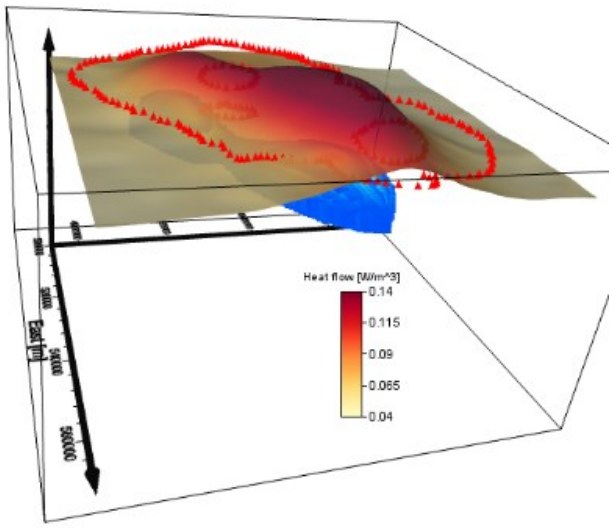

Figure 27. Heat flux computed at the surface of the volume

Even though fumaroles at Yellowstone have far lower temperatures than at many volcanoes, thousands of boiling thermal features dot the landscape and cover about 70 km² (out of 9000 km² in the park) (Lowenstern et al, 2006). Probably the most convincing evidence for a relatively shallow magma body is the immense heat flow issuing from Yellowstone on a continuous basics (Figure 28). Figure (28), represents some profiles done in order to map the heat flow at the surface and the temperature distribution of the volume along the caldera: the temperature, as I have shown before, ranges from 0 °C at the surface to about 1150 °C at the bottom of the model. The heat flow profiles show the maximum value (0.15 W/m²) exactly above the caldera and then it significantly decreases. The iso-Curie surface which I deduced from the previous comparison with the spectral analysis iso-Curie surface result can be set around 500 °C, in all the profiles a purple contour lines interval is highlighted in order to give a range of temperature where the Curie surface can be: the Iso-Curie surface is definitely above the magmatic chamber whose presented in the profiles and especially well manifested in the N-S profiles (along Y coordinates). It is well shown that the temperature in the magmatic chamber is ranging from 700 °C to 750 °c - 800°C.

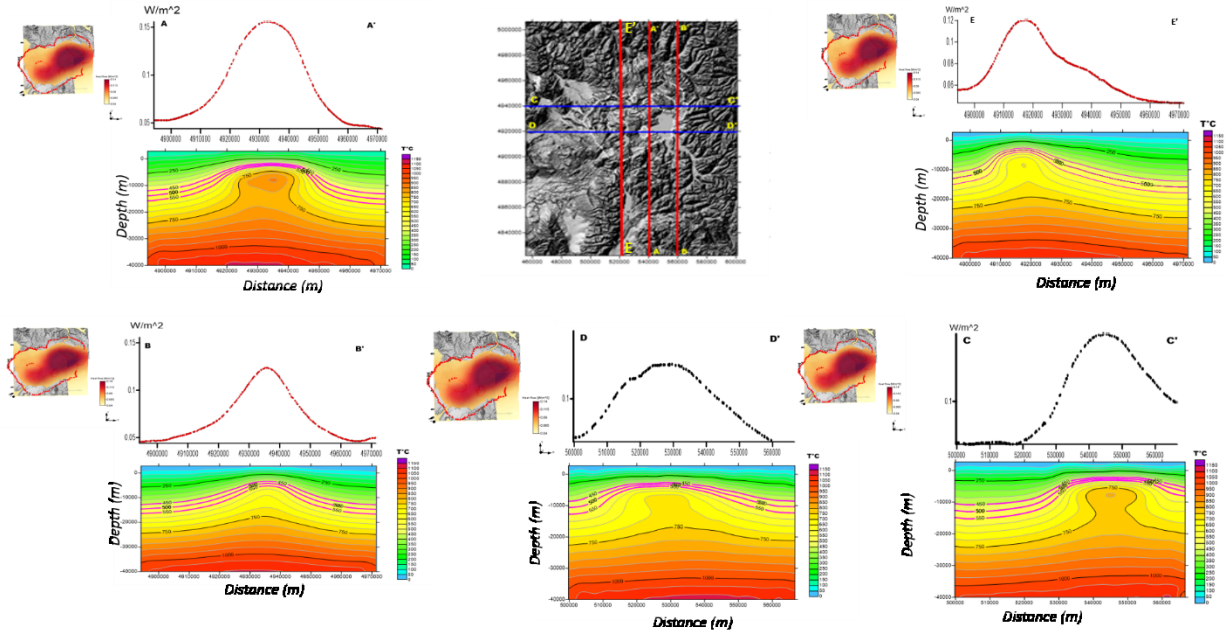

Figure 28. Profiling the temperature and the heat flow along the caldera

5.4. 3D Rheological Model

The long-time rheological behaviour of the lithosphere is strongly dependent upon temperature. For T<T*, where T* depends on the material under consideration, the behaviour is brittle. At higher temperature, the behaviour is ductile. Brittle behaviour, in a static sense, is adequately described by the Columb-Navier shear failure criterion (e.g. Jaeger and Cook, 1979; Ranalli, 1995).

The ductile deformation a result of a low-frequency behaviour (Figure 29), is governed by (Kirby, 1983):

$$(\sigma_1 - \sigma_3)_D = (\dot{\varepsilon}/A)^{1/n} \, exp\left({}^{Q}/_{nRT}\right) \qquad (5.4)$$

where:

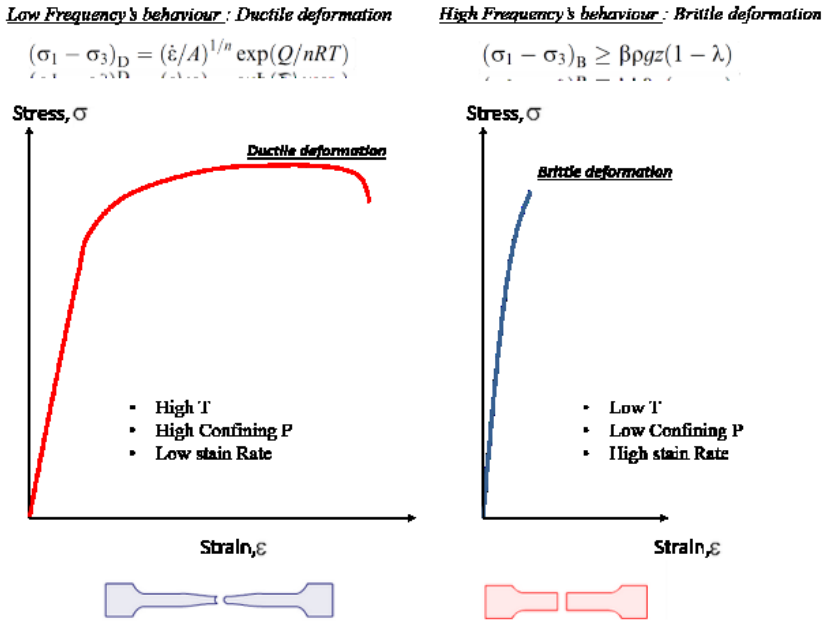

Figure 29. Representations & Equations of the Brittle and Ductile behaviour

Although, the brittle deformation express a high-frequency behaviour (Figure 29), which is governed by (Sibson, 1974):

$$(\sigma_1 - \sigma_3)_D \geq \beta\rho gz(1-\lambda) \qquad (5.5)$$

Where $\sigma_1 - \sigma_3$ measured in Pa is the stress difference required to maintain the steady-state strain rate ε, g is the acceleration of gravity, z the depth in m, R is the gas constant measured in , T is the temperature, λ the pore fluid factor, β is the type of faults ranging from 0.75 to 3 (3.0 for the thrust, 1.2 for the strike-slip and 0.75 for the normal faulting), ρ is the rock density measured (kg/m^3); λ is the pore factor and A, the pre-exponential of Arrhenius equation (MPa^{-n} s^{-1}), n mole and Q (KJ/mol) the energy activation for the creep and represents the properties of the rocks.

The brittle-ductile transition could be retrieved by a comparison between (Equation 5.4) and (Equation 5.5). A very important information like the rheological model could be obtained: The Brittle-Ductile (B/D) transition in the crust is thought to be related to the seismic– aseismic boundary.

For instance, Solaro et al. (2010) performed a rheological model along a WSW–ENE-oriented cross-section running from Neapolitan Volcanic Zone to Apulia foreland, Italy. This study gave a continuous solution showing that the area is characterized by horizontal rheological variations, with two horizons interlayered with ductile horizons, which are quite predominant with respect to the vertical ones.

While Solaro et al (2010) have done their study using rheological profile along a section that goes from the Neapolitan volcanic area to Puglia crossing the Apennine (Italy), Denosaquo et al., (2009), calculated the strength envelop in just three discrete points.

This latter, computed the strength profile (Figure 30) of the Plane River Snake including Yellowstone, but in certain points: the eastern Snake River Plain (SRP), Yellowstone Plateau (YP), and Yellowstone caldera (YC).

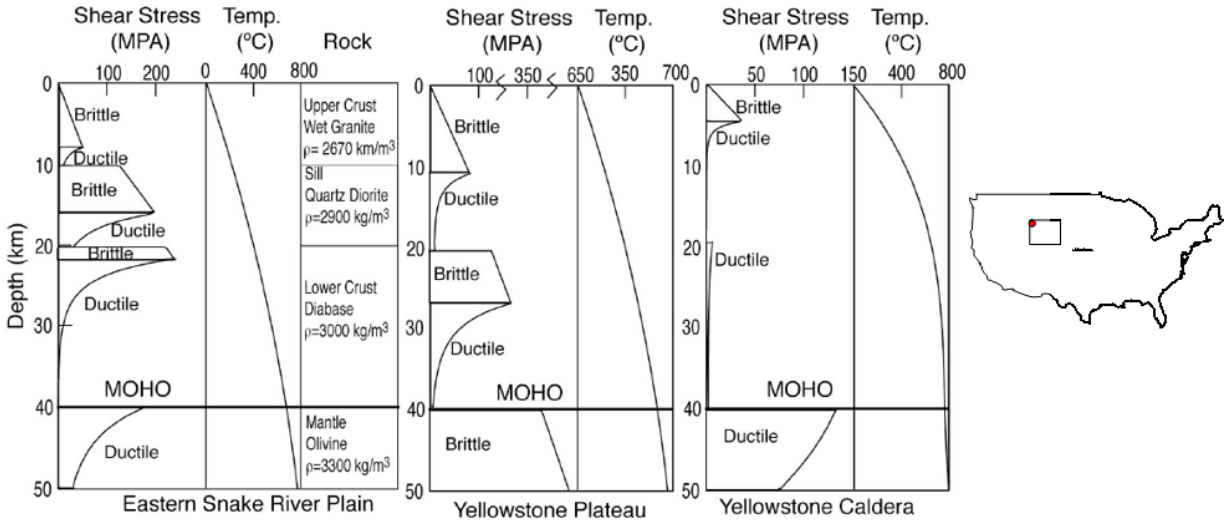

Figure 30. Strength models of the eastern SRP, Yellowstone Plateau, and Yellowstone caldera (after Denasoquo et al., 2009).

These locations represent the track of the Yellowstone hotspot, the area immediately adjacent to the active volcanic system, and the active volcanic system itself. In the eastern Snake River Plane, the brittle-ductile transition for granite occurs at about 8 km. The Snake River Plane mid-crustal sill is brittle to about 16 km depth, and the lower crust is entirely ductile. The brittle-ductile transition in the lower crust occurs at about 21 km and the mantle is entirely ductile. In the Yellowstone plateau the brittle-ductile transition occurs at about 11 km.

A brittle-ductile transition occurs in the lower crust at about 27 km. The upper mantle behaves as a brittle medium as well. Inside the Yellowstone caldera the brittle-ductile transition occurs at about 4 km. The lower crust and upper mantle are both ductile. In the eastern Snake River Plane and the Yellowstone Plateau the lower crust is partially brittle.

Based on the geological and the thermal information I already retrieved in section 5.3, a 3D rheological model was computed considering a $\beta = 0.75$, through which I investigated our B/D transition zone for different time scales 10^8 years ($\varepsilon = 10^{-8}\ s^{-1}$), corresponding to recent dynamic of the Yellowstone caldera (Figure 31) and 10^{13} years ($\varepsilon = 10^{-13}\ s^{-1}$), corresponding to

the time evolution of the caldera (Figure 32). Both models agree well with the present distribution of earthquakes (Figure 34a,b).

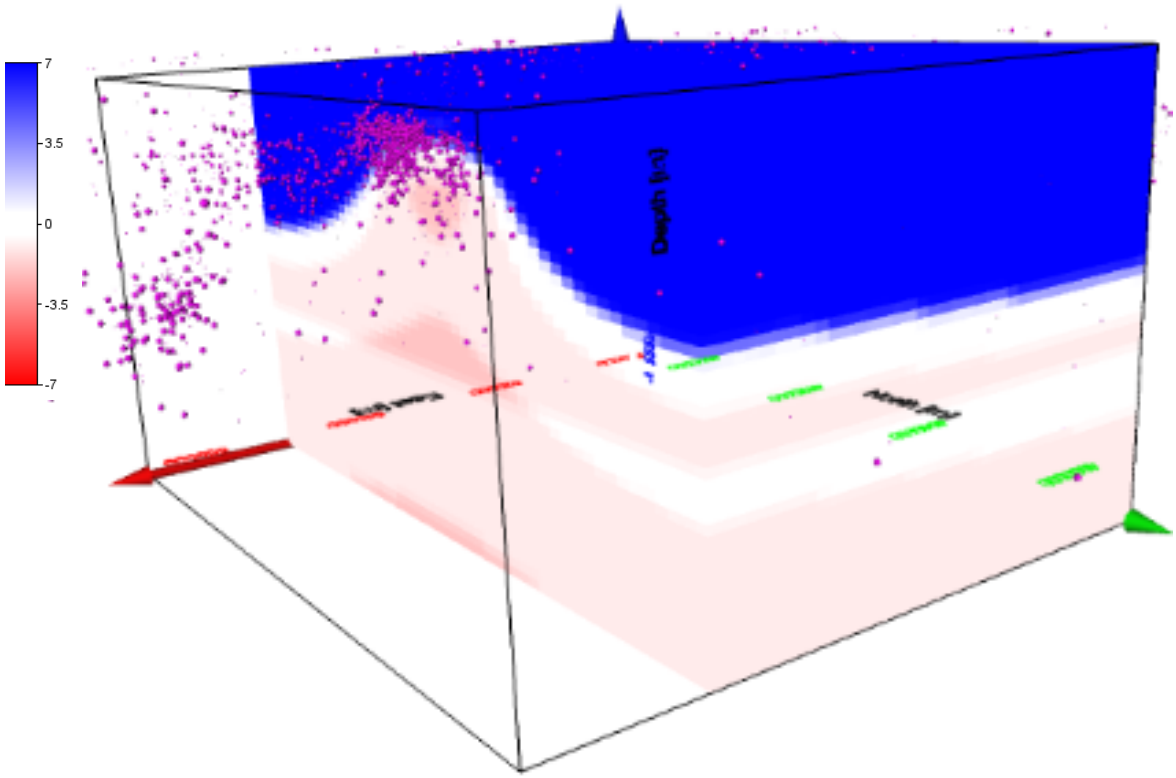

Figure 31. The brittle- ductile volume distribution for a strain rate of $10^{-8}s^{-1}$.

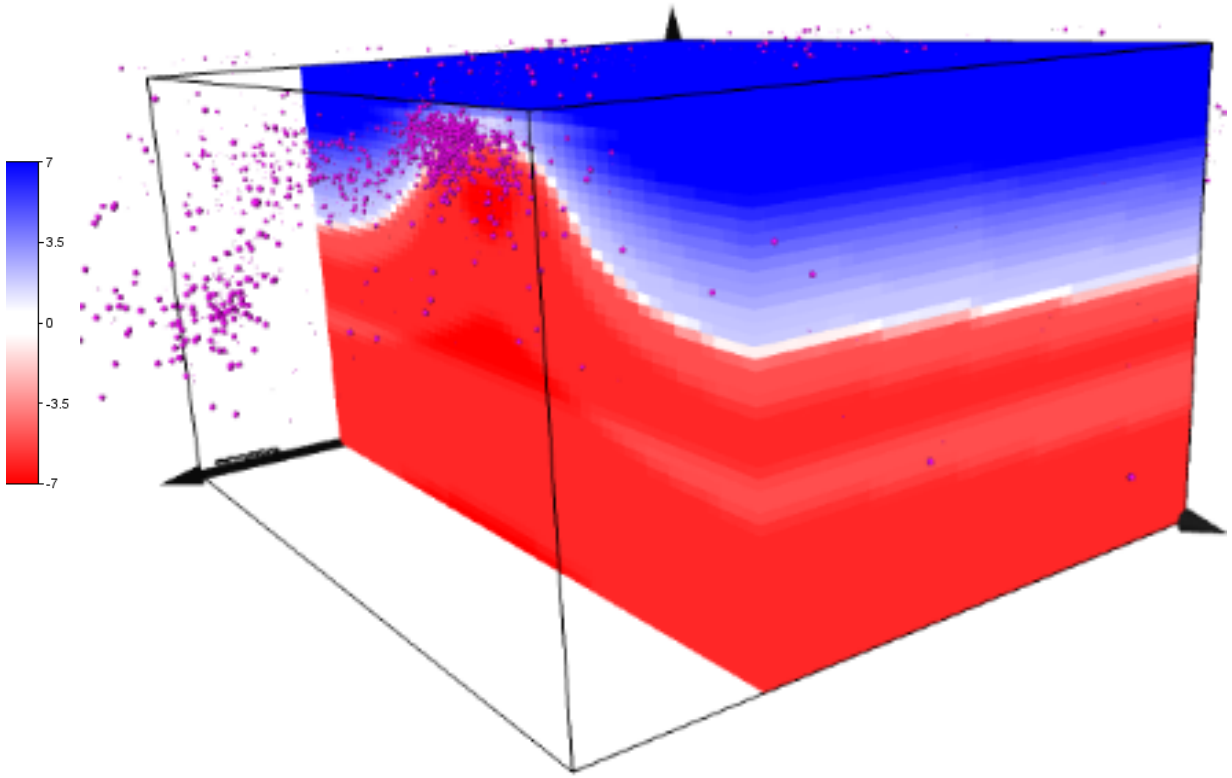

Figure 32. Brittle-Ductile volume modeled for a strain rate of 10^{-13} s^{-1}.

5.5. Rheology and natural seismicity

The Yellowstone Plateau is one of the most seismically active areas of the western U.S. and is part of the distinct N–S band of intraplate seismicity known as the Intermountain seismic belt (Smith and Sbar, 1974; Smith and Arabasz, 1991). Overall, seismic activity in Yellowstone is characterized by swarms of small, shallow earthquakes (Farrell et al., 2014).

The earthquake data used in this study (Figure 33) are from the University of Utah Seismic Stations (UUSS) catalog from 1996 to 2014 (Farrell et al., 2014), and the earthquake from 2014 to 2017 were a personal communication from Dr. Jamie Farrell. Most of the seismicity is concentrated in the northeastern part of Yellowstone caldera.

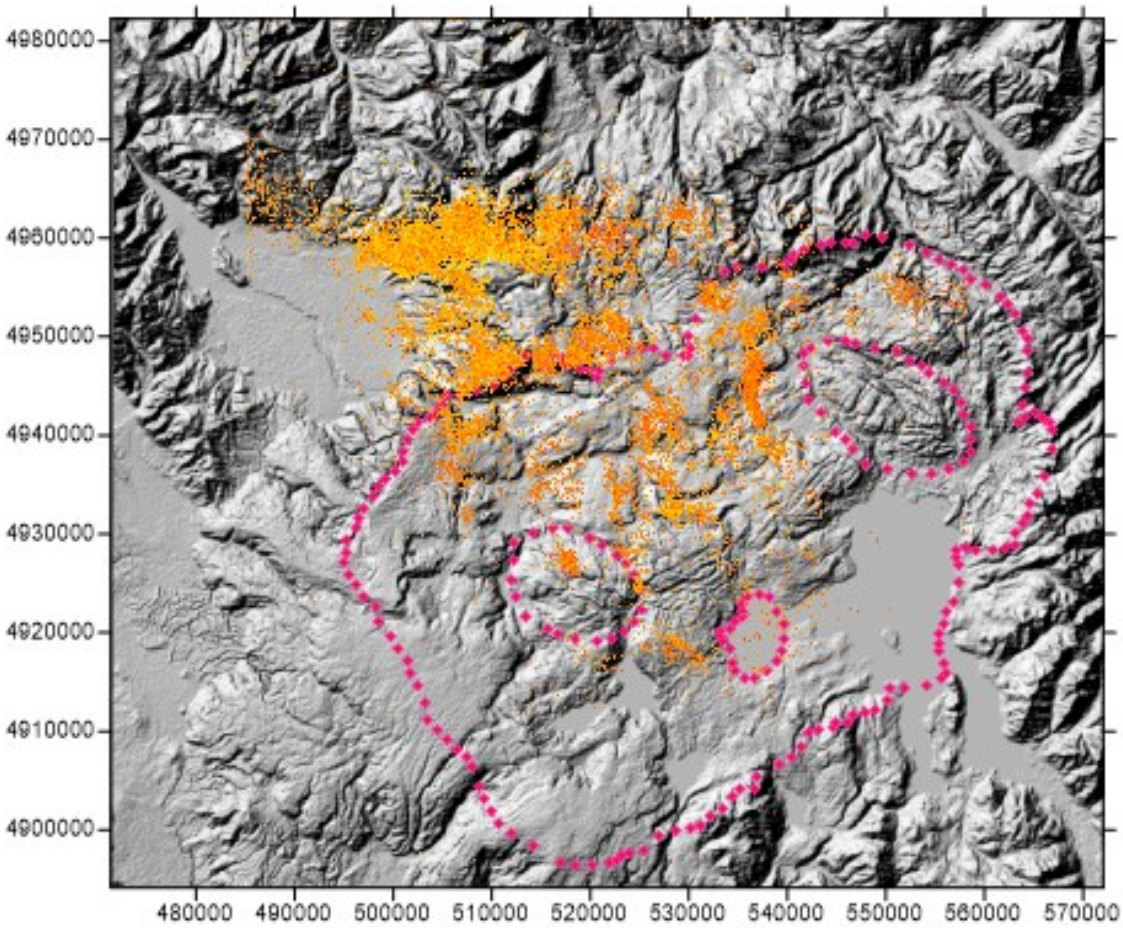

Figure 33. Earthquakes distribution on Yellowstone (The pink point limit represent the caldera limits); the 33,696 events are collected from 1996-2017 with a maximum magnitude 4.8

Focal depths within the Yellowstone caldera are very shallow, limited by high temperature, indeed they are located at 4-6 km of depth where the brittle-ductile transition exists. The latter deepens up to 18 km in the much cooler tectonic regime in the Hebgen Lake, MT area west of the caldera (Smith et al., 2009)

About 33,696 earthquakes were recorded, with the highest magnitude is 4.8 and is located outside the caldera. The acquired depths are ranging from 0.2 km inside the caldera to 10 km outside the caldera.

Figure (35) represents the histograms of number of earthquakes along the caldera in the same direction of the Brittle-Ductile profiles (e.g. Figure 34.a; Figure 34.b); most of the earthquakes are concentrated in the upper part of the crust (the first 4 km), as also confirmed by the ductile behaviour of the crust and the high temperature.

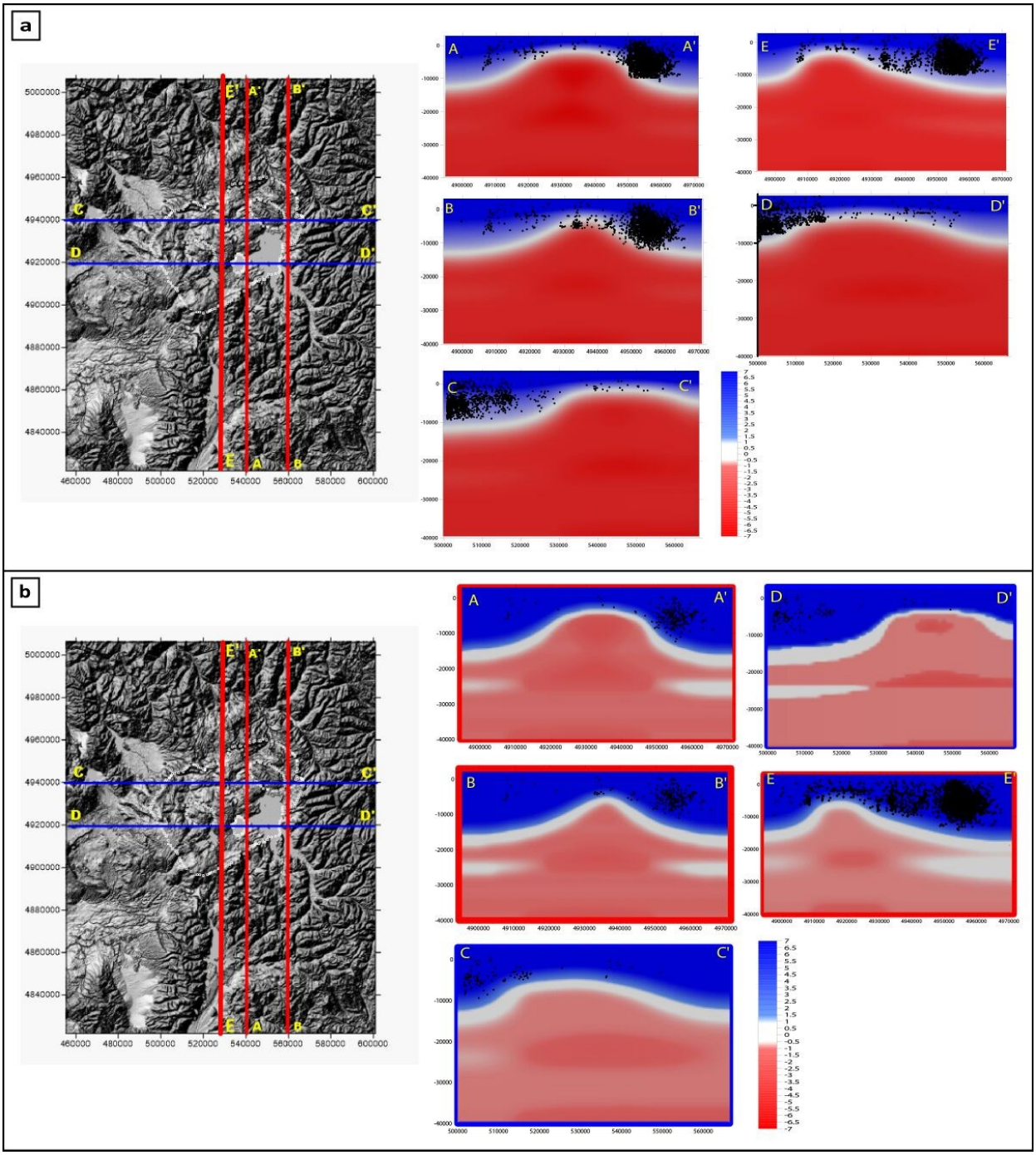

Figure 34. Both figures represent the earthquakes distribution a) Cross sections along the caldera with a strain rate of 10^{8}; b) Cross sections along the caldera representing the results of 10^{13} strain

Figure 34 (a, b.), represents the mapping of the Brittle-Ductile behaviour of the crust under Yellowstone caldera for a strain rate of $10^{-8}\ s^{-1}$ and $10^{-13}\ s^{-1}$ respectively. We can notice that the earthquake distribution in the Figure (34 a) does not reach the transition, being do not go to the transition (Figure 35), being concentrated in the brittle region while the Figure (34 b)

evidences that the earthquakes in some locations go beyond the brittle domain. This finding confirms the validity of the computed rheological model.

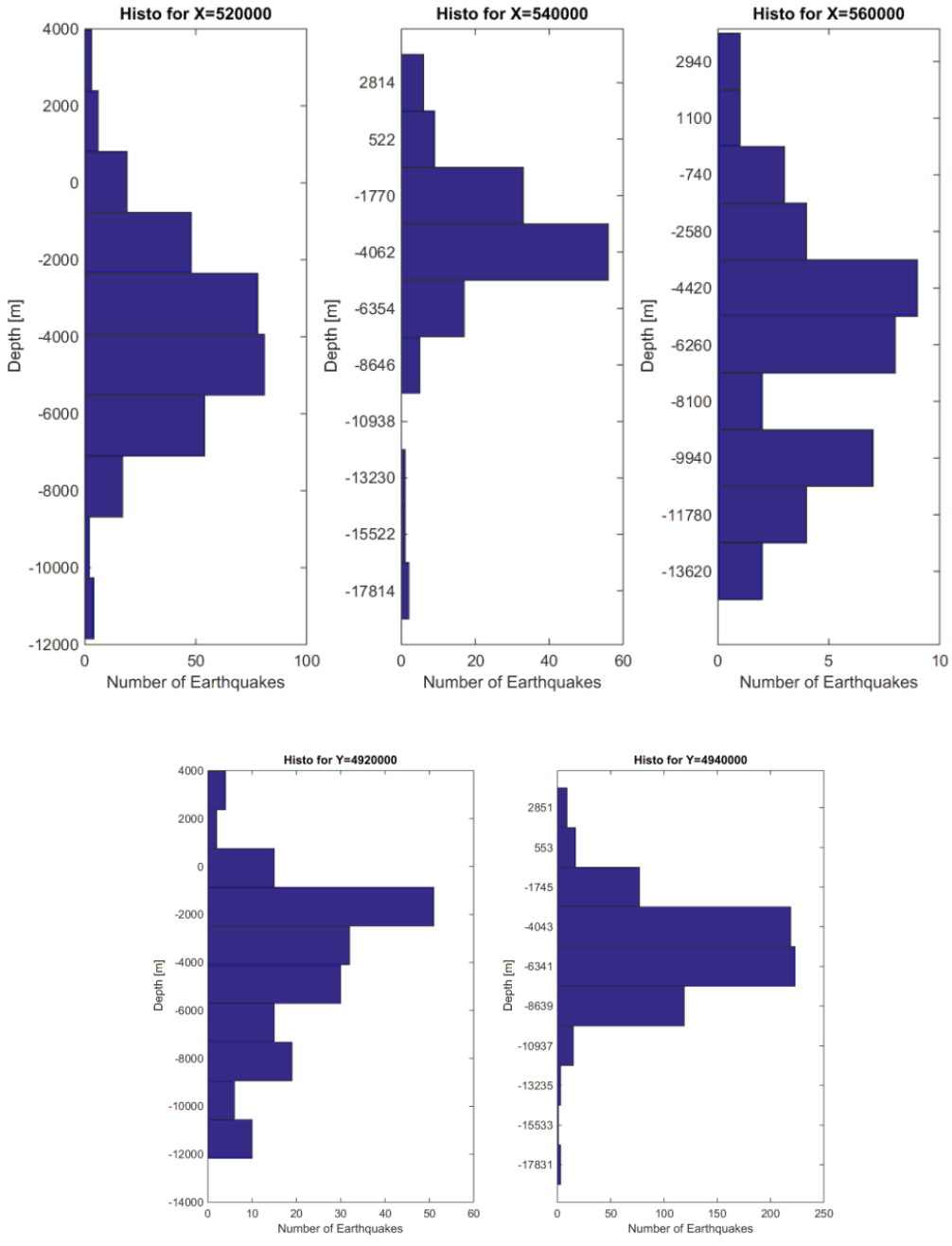

Figure 35. Histograms of number of earthquakes vs depths along the caldera

5.6. Discussions & Conclusions

In order to investigate the rheological features of the crust beneath Yellowstone caldera, I performed a 3D thermal model followed by a 3D rheological model. To do this, I performed a 3D finite element stationary conductive model, by inverting the tomography model, and optimizing the geothermal heat source parameters.

I was able to characterize the structural domains in terms of thermal variations and Brittle–Ductile behaviour. In this contest, I generated several forward models consisting in a 3D stationary conductive solution of the thermal regime of the crust beneath Yellowstone caldera.

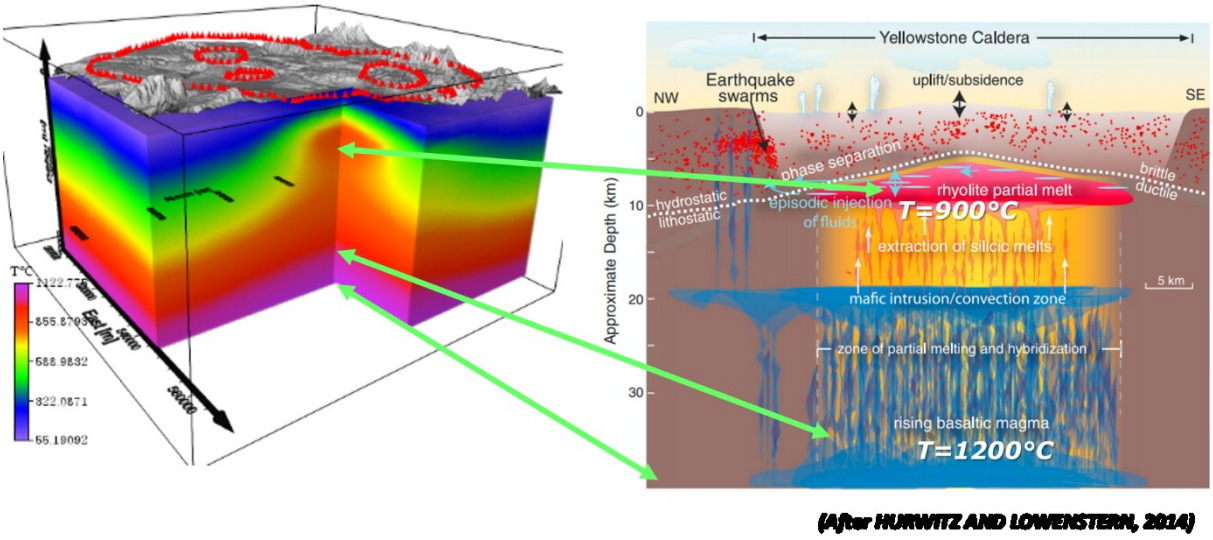

Figure 36. Comparison between the computed 3D thermal model and the model built by Hurwitz and Lowenstern (2014)

I remark that the achieved results, relevant to the temperature distribution and the heat flow distribution, are also in agreement with previous studies (e.g. Hurwitz and Lownstern, 2014; smith et al., 2009; Farrell et al., 2014) (Figure 36).

Finally, I use of the depth distribution of the iso-Curie surface computed using spectral analysis methods from aeromagnetic data, and a full earthquakes catalog to constrain and to validate our results.

The absence of the deep geothermal well data were replaced by the presence of the few yet, representing heat flow measurements that converge with our heat flow result.

Conclusions and future perspectives

The study has different aspects to the purpose of making the analysis and the understanding of the rheological crust under volcanic areas and in particular Yellowstone caldera. Many reasons were behind the choice of Yellowstone caldera as a study area, for instance:

- Yellowstone, as many scientist described it, is a geological smoking gun that illustrates how violent the Earth can be.
- It is an explosive supervolcano where many studies have proven that beneath it lies a hot, upwelling plume of mantle.
- It is characterized by a very high heat flow yet there is no quantification of the brittle ductile transition in that area.

And countless other reasons. The eruption at Yellowstone 2.1 Ma ago, released 2,450 cubic kilometres of material. The last eruption at Yellowstone which was 640,000 years ago released 1,000 cubic kilometres of material; such an eruption at Yellowstone would have catastrophic consequences.

The purposes of this work are (i) to give an estimation of the depth to the iso-Curie surface and (ii) to portray a full three-dimension image of the thermal situation as well as the rheological behaviour of the crust under Yellowstone.

To investigate the depth to the Iso-Curie surface under Yellowstone, a comparison between two Spectral analysis methods (Fractal analysis, and the corrected Spector and Grant method) was performed; although, they use different approaches and assumptions, they do basically have the same limitations. Moreover, the estimation of the most suitable fractal sloping exponent led to a value equal to the fixed sloping exponent of the corrected Spector and Grant method.

The results achieved from using these methods have the same range of depths (from 1 km to 5 km), and relatively the same distributions. The shallowest depths are located inside the caldera and the deepest ones are located everywhere else.

A 3D thermal model was constructed through solving a 3D finite element problem of heat transfer in a conductive system using Comsol Multiphysics software, involving a trial and error optimization of the density, velocity models jointly with the geothermal heat source parameters. The obtained depth to the Curie map was a key constraint parameter to check the validity of the thermal model.

Subsequently, a 3D rheological model was built with the 3D temperature model as an input along with the geological and the geophysical information from literature. The most part of earthquakes epicentres were found to be concentrated in the brittle zone of the volume while the ductile zone is not totally homogeneous confirming the sandwich theory of the crust suggested by different authors (e.g. Ranalli, 1997); this Brittle-Ductile volume is the first 3D mapping of the rheological features of the crust under Yellowstone caldera.

Regarding the future perspectives, I recommend investigating the deformation field under Yellowstone caldera in order to have a third-part information. As mentioned above, the Yellowstone caldera, represents a key opportunity to evaluate the geodynamics processes activities in a continental hotspot and its interaction with a continental plate.

Investigating the crust using the Differential Interferometric Synthetic-Aperture Radar (DInSAR) ground deformation data could be an important advantage to our results.

I also recommend investigating the ability of this ground deformation field to be considered as a potential field (Brahmi et al., 2017), by using the elastic rheology model. And in this scenario, considering the elastic field theory under the Boussinesq (1885) and Love (1892) approximations, methods such as the CWT (Fedi., 2007; Fedi et al., 2009) and the Euler Deconvolution, will allow investigation of the sources' features responsible of the recorded active deformation, so enhancing the rheological model of the Yellowstone volcano.

References

Arnet, F., Kahle, H. G., Klingelé, E., Smith, R. B., Meertens, C. M., & Dzurisin, D. (1997). Temporal gravity and height changes of the Yellowstone caldera, 1977–1994. Geophysical Research Letters, 24(22), 2741-2744.

Bansal A. R., Gabriel G., Dimri V. P., and Krawczyk C. M., (2011). "Estimation of depth to the bottom of magnetic sources by a modified centroid method for fractal distribution of sources: An application to aeromagnetic data in Germany," Geophysics, vol. 76, no. 3, p. L11, 2011.

Battaglia, M., & Hill, D. P. (2009). Analytical modeling of gravity changes and crustal deformation at volcanoes: The Long Valley caldera, California, case study. Tectonophysics, 471(1), 45-57.

Battaglia, M., Segall, P., & Roberts, C. (2003). The mechanics of unrest at Long Valley caldera, California. 2. Constraining the nature of the source using geodetic and micro-gravity data. Journal of Volcanology and Geothermal Research, 127(3), 219-245.

Bansal, A. R., & Dimri, V. P. (1999). Gravity evidence for mid crustal domal structure below Delhi fold belt and Bhilwara super group of western India. Geophysical Research Letters, 26(18), 2793-2795.

Bansal, A. R., Gabriel, G., Dimri, V. P., & Krawczyk, C. M. (2011). Estimation of depth to the bottom of magnetic sources by a modified centroid method for fractal distribution of sources: An application to aeromagnetic data in Germany. Geophysics, 76(3), L11-L22.

Bhattacharyya, B. K., & Leu, L. K. (1975). Analysis of magnetic anomalies over Yellowstone National Park: Mapping of Curie point isothermal surface for geothermal reconnaissance. Journal of Geophysical Research, 80(32), 4461-4465.

Bhattacharyya, B. K. (1966). Continuous spectrum of the total-magnetic-field anomaly due to a rectangular prismatic body. Geophysics, 31(1), 97-121.

Blakely, R.J., 1996. Potential theory in gravity and magnetic applications. Cambridge Univ. Press, 441.

Bouligand, C., Glen, J. M., & Blakely, R. J. (2009). Mapping Curie temperature depth in the western United States with a fractal model for crustal magnetization. Journal of Geophysical Research: Solid Earth, 114(B11).

Boussinesq, M.J. (1885).Application des potentiels a l'étude de l'équilibre et du mouvement des solides élastiques, avec des notes étendues sur divers points de physique mathé- matique et d'analyse. Paris: Gauthier-Villard imprimeur libraire.

Brahmi, M., Castaldo, R., Barone, A., Fedi, M., & Tizzani, P. (2017, April). Solving Laplace equation to investigate the volcanic ground deformation pattern. In EGU General Assembly Conference Abstracts (Vol. 19, p. 946).

Castaldo, R., Gola, G., Santilano, A., De Novellis, V., Pepe, S., Manzo, M., Manzella, A., & Tizzani, P. (2017). The role of the thermo-rheological properties of the crust beneath Ischia Island (Southern Italy) in the modulation of the ground deformation pattern. Journal of Volcanology and Geothermal Research 344, 154–173.

Chiozzi, P., Matsushima, J., Okubo, Y., Pasquale, V., & Verdoya, M. (2005). Curie-point depth from spectral analysis of magnetic data in central–southern Europe. Physics of the Earth and Planetary Interiors, 152(4), 267-276.

Dimri, V. P. (2000). Crustal fractal magnetization. Application of Fractals in Earth Sciences. 1st ed. Oxford, UK: IBH Publishing Co, 89-95.

Chang, W. L., Smith, R. B., Farrell, J., & Puskas, C. M. (2010). An extraordinary episode of Yellowstone caldera uplift, 2004–2010, from GPS and InSAR observations. Geophysical Research Letters, 37(23).

Chang, W. L., Smith, R. B., Wicks, C., Farrell, J. M., & Puskas, C. M. (2007). Accelerated uplift and magmatic intrusion of the Yellowstone caldera, 2004 to 2006. Science, 318(5852), 952-956.

Christiansen, R. L. (2001). The Quaternary and pliocene Yellowstone plateau volcanic field of Wyoming, Idaho, and Montana (No. 729-G).

Christiansen, R. L., & Blank Jr, H. R. (1972). Volcanic stratigraphy of the Quaternary rhyolite plateau in Yellowstone National Park (No. 729-B). US Geological Survey.

Christiansen, R.L., & Blank, H.L. (1974). Geologic map of the Old Faithful quadrangle, Yellowstone National Park, Wyoming: U.S. Geological Survey Geologic Quadrangle Map GQ-1189, scale 1:62,500.

Christiansen, R.L., & Lipman P.W. (1972). Cenozoic volcanism and plate-tectonic evolution of the Western United States: Part 2, Late Cenozoic: Royal Society of London Philosophical Transactions, ser. A, 271, 249-284.

Christiansen, R. L. (2001). The Quaternary and pliocene Yellowstone plateau volcanic field of Wyoming, Idaho, and Montana (No. 729-G).

DeNosaquo, K. R., Smith, R. B., & Lowry, A. R. (2009). Density and lithospheric strength models of the Yellowstone–Snake River Plain volcanic system from gravity and heat flow data. Journal of Volcanology and Geothermal Research, 188(1), 108-127.

Dolmaz, M. N., Hisarli, Z. M., Ustaömer, T., & Orbay, N. (2005). Curie point depths based on spectrum analysis of aeromagnetic data, West Anatolian extensional province, Turkey. Pure and applied geophysics, 162(3), 571-590.

Dvorak, J. J., & Dzurisin, D. (1997). Volcano geodesy: The search for magma reservoirs and the formation of eruptive vents. Reviews of Geophysics, 35(3), 343-384

Dzurisin, D. (2003). A comprehensive approach to monitoring volcano deformation as a window on the eruption cycle. Reviews of Geophysics, 41(1).

Dzurisin, D., Wicks Jr, C., & Thatcher, W. (1999). Renewed uplift at the Yellowstone Caldera measured by leveling surveys and satellite radar interferometry. Bulletin of Volcanology, 61(6), 349-355.

Dzurisin, D., Yamashita, K. M., & Kleinman, J. W. (1994). Mechanisms of crustal uplift and subsidence at the Yellowstone caldera, Wyoming. Bulletin of Volcanology, 56(4), 261-270.

Eletta, B. E., & Udensi, E. E. (2012). Investigation of the Curie point isotherm from the magnetic fields of eastern sector of central Nigeria. Geosciences, 2(4), 101-106.

Ellis, A. J., & Wilson, S. H. (1955). The heat from the Wairakei-Taupo thermal region calculated from the chloride output. New Zealand Journal of Science and Technology B, General Research Section, 36, 622-631.

Evans, W. C., Bergfeld, D., McGeehin, J. P., King, J. C. & Heasler, H. (2010). Tree-ring 14C links seismic swarm to CO2 spike at Yellowstone, USA. Geology, 38, 1075-1078. doi:doi: 10.1130/â€'G31345.1 http://geology.geoscienceworld.org/content/38/12/1075.abstract

Farrell, J., Smith, R. B., Husen, S., & Diehl, T. (2014). Tomography from 26 years of seismicity revealing that the spatial extent of the Yellowstone crustal magma reservoir extends well beyond the Yellowstone caldera. Geophysical Research Letters, 41(9), 3068-3073.

Farrell, J., Smith, R. B., Taira, T., Chang, W. & Puskas, C. M. (2010). Dynamics and rapid migration of the energetic 2008-2009 Yellowstone Lake earthquake swarm. Geophysical Research Letters, 37 doi:10.1029/2010GL044605

Farrell, J., Smith, R. B., Husen, S., & Diehl, T. (2014). Tomography from 26 years of seismicity revealing that the spatial extent of the Yellowstone crustal magma reservoir extends well beyond the Yellowstone caldera. Geophysical Research Letters, 41(9), 3068-3073.

Fedi, M., (2007). DEXP: a fast method to determine the depth and the structural index of potential fields sources, Geophysics, 72(1), I1–I11,doi:10.1190/1.2399452.

Fedi M. (2016). Scaling Laws in Geophysics: Application to Potential Fields of Methods Based on the Laws of Self-similarity and Homogeneity. In: Dimri V. (eds) Fractal Solutions for Understanding Complex Systems in Earth Sciences. Springer Earth System Sciences. Springer, Cham

Fedi, M., Cella, F., Quarta, T., & Villani, A. V. (2010). 2D continuous wavelet transform of potential fields due to extended source distributions. Applied and Computational Harmonic Analysis, 28(3), 320-337.

Fedi M, Florio G and Quarta T. (2009) Multiridge analysis of potential fields: Geometric method and reduced Euler deconvolution, GEOPHYSICS, VOL. 74, NO. 4 JULY-AUGUST 2009; P. L53–L65, 15 FIGS, 1TABLE. 10.1190/1.31427222

Fedi, M., Quarta, T., & De Santis, A. (1997). Inherent power-law behavior of magnetic field power spectra from a Spector and Grant ensemble. Geophysics, 62(4), 1143-1150.

Finn, C. A., & Morgan, L. A. (2002). High-resolution aeromagnetic mapping of volcanic terrain, Yellowstone National Park. Journal of Volcanology and Geothermal Research, 115(1), 207-231.

Fournier, R. O. (1989). Geochemistry and dynamics of the Yellowstone National Park hydrothermal system. Annual Review of Earth and Planetary Sciences, 17(1), 13-53.

Gates, A. E., & Ritchie, D. (2007). Encyclopedia of Earthquakes and Volcanoes Facts on File. New York.

Fournier, R. O., White, D. E., & Truesdell, A. H. (1976). Convective heat flow in Yellowstone National Park. In Proceedings of the 2nd UN Symposium on the Development and Use of Geothermal Resources, San Francisco (pp. 731-739).

Gardner, G. H. F., Gardner, L. W., & Gregory, A. R. (1974). Formation velocity and density—The diagnostic basics for stratigraphic traps. Geophysics, 39(6), 770-780.

Grauch, V.J.S., & Millegan, S. (1998). Mapping intrabasinal faults from high-resolution aeromagnetic data. Leading Edge 17, 53-55.

Hildreth, W., Christiansen, R. L., & O'Neil, J. R. (1984). Catastrophic isotopic modification of rhyolitic magma at times of caldera subsidence, Yellowstone Plateau volcanic field. Journal of Geophysical Research: Solid Earth, 89(B10), 8339-8369.

Hill, D.P., 1998, 1998 Seismological Society of America Meeting-Presidential Address: Science, geologic hazards, and the public in a large restless caldera: Seismological Research Letters, v. 69, no. 5, p. 400-404.

Hill, D. P. (2006). Unrest in Long Valley Caldera, California, 1978–2004. Geological Society, London, Special Publications, 269(1), 1-24.

Huang, H. H., Lin, F. C., Schmandt, B., Farrell, J., Smith, R. B., & Tsai, V. C. (2015). The Yellowstone magmatic system from the mantle plume to the upper crust. Science, 348(6236), 773-776.

Hurwitz, S., Christiansen, L. B., & Hsieh, P. A. (2007). Hydrothermal fluid flow and deformation in large calderas: Inferences from numerical simulations. Journal of Geophysical Research: Solid Earth, 112(B2).

Hurwitz, S., & Lowenstern, J. B. (2014). Dynamics of the Yellowstone hydrothermal system. Reviews of Geophysics, 52(3), 375-411.

Hutnak, M., Hurwitz, S., Ingebritsen, S. E., & Hsieh, P. A. (2009). Numerical models of caldera deformation: Effects of multiphase and multicomponent hydrothermal fluid flow. Journal of Geophysical Research: Solid Earth, 114(B4).

Jaworowski, C., Heasler, H. P., Neale, C. M., & Sivarajan, S. (2010). Using thermal infrared imagery and LiDAR in Yellowstone geyser basins. Yellowstone Science, 18(1), 8-19.

Jaeger, J. C., & Cook, N. G. W. (1979). Fundamentals of rock mechanics, 593 pp.

Jiaxiang, Z. H. T. (1998). A Three Dimensional Finite Element Model of Cable Stayed Bridges for Dynamic Analysis [J]. JOURNAL OF VIBRATION ENGINEERING, 1.

Karastathis, V. K., Papoulia, J., Di Fiore, B., Makris, J., Tsambas, A., Stampolidis, A., & Papadopoulos, G. A. (2010, June). Exploration of the deep structure of the central Greece geothermal field by passive seismic and Curie depth analysis. In 72nd EAGE Conference and Exhibition incorporating SPE EUROPEC 2010.

Kirby, S. H. (1983). Rheology of the lithosphere. Reviews of Geophysics, 21(6), 1458-1487.

Lanza, R., & Meloni, A. (2006). The Earth's magnetism. Springer-Verlag Berlin Heidelberg.

Langel, R. A., & Hinze, W. J. (1998). The magnetic field of the Earth's lithosphere: The satellite perspective. Cambridge University Press.

Lanphere, M. A., Champion, D. E., Christiansen, R. L., Izett, G. A., & Obradovich, J. D. (2002). Revised ages for tuffs of the Yellowstone Plateau volcanic field: Assignment of the Huckleberry

Ridge Tuff to a new geomagnetic polarity event. Geological Society of America Bulletin, 114(5), 559-568.

Lehman, J. A., Smith, R. B., Schilly, M. M., & Braile, L. W. (1982). Upper crustal structure of the Yellowstone caldera from seismic delay time analyses and gravity correlations. Journal of Geophysical Research: Solid Earth, 87(B4), 2713-2730.

Lindseth, R. O. (1979). Synthetic sonic logs—A process for stratigraphic interpretation. Geophysics, 44(1), 3-26.

Lowenstern, J. B., & Hurwitz, S. (2008). Monitoring a supervolcano in repose: Heat and volatile flux at the Yellowstone Caldera. Elements, 4(1), 35-40.

Love A.E.H. (1892). A treatise on the mathematical theory of elasticity, second edition – Cambridge Press, 1906

Maus, S., & Dimri, V. P. (1994). Scaling properties of potential fields due to scaling sources. Geophysical Research Letters, 21(10), 891-894.

Maus, S., Gordon, D., & Fairhead, D. (1997). Curie-temperature depth estimation using a self-similar magnetization model. Geophysical Journal International, 129(1), 163-168.

Meertens, C. M., & Smith, R. B. (1991). Crustal deformation of the Yellowstone caldera from first GPS measurements: 1987–1989. Geophysical research letters, 18(9), 1763-1766.

Obande, G. E., Lawal, K. M., & Ahmed, L. A. (2014). Spectral analysis of aeromagnetic data for geothermal investigation of Wikki Warm Spring, north-east Nigeria. Geothermics, 50, 85-90.

Okubo, Y., Graf, R. J., Hansen, R. O., Ogawa, K., & Tsu, H. (1985). Curie point depths of the island of Kyushu and surrounding areas, Japan. Geophysics, 50(3), 481-494.

Pelton, J. R., & Smith, R. B. (1982). Contemporary vertical surface displacements in Yellowstone National Park. Journal of Geophysical Research: Solid Earth, 87(B4), 2745-2761.

Pierce, K. L., K. P. Cannon, G. A. Meyer, M. J. Trebesch, & R. D. Watts (2002), Post-Glacial Inflation-Deflation Cycles, Tilting, and Faulting in the Yellowstone Caldera Based on Yellowstone Lake Shorelines, U.S. Geol. Surv. Open File Rep., 2002-142.

Pilkington, M., & Todoeschuck, J. P. (1990). Stochastic inversion for scaling geology. Geophysical Journal International, 102(1), 205-217.

Pilkington, M., Gregotski, M. E., & Todoeschuck, J. P. (1994). Using fractal crustal magnetization models in magnetic interpretation. Geophysical prospecting, 42(6), 677-692.

Pilkington, M., & Todoeschuck, J. P. (1993). Fractal magnetization of continental crust. Geophysical Research Letters, 20(7), 627-630.

Piskarev, A. and Elkina, D., 2017. Giant caldera in the Arctic Ocean: Evidence of the catastrophic eruptive event. Scientific Reports, 7.

Quarta, T., Fedi, M., & De Santis, A. (2000). Source ambiguity from an estimation of the scaling exponent of potential field power spectra. Geophysical Journal International, 140(2), 311-323.

Rajaram, M. (2007). Depth to Curie temperature. In Encyclopedia of Geomagnetism and Paleomagnetism (pp. 157-159). Springer Netherlands.

Ranalli, G. (1995). Rheology of the Earth. Springer Science & Business Media.

Ranalli, G. (1997). Rheology of the lithosphere in space and time. Geological Society, London, Special Publications, 121(1), 19-37.

Saleh, S., Salk, M., & Pamukçu, O. (2013). Estimating Curie point depth and heat flow map for northern Red Sea rift of Egypt and its surroundings, from aeromagnetic data. Pure and applied geophysics, 170(5), 863-885

Shen, W., M. Ritzwoller, and V. Schulte-Pelkum (2013b), A 3-d model of the crust and uppermost mantle beneath the central and western US by joint inversion of receiver functions and surface wave dispersion, J. Geophys. Res., 60, 1–15.

Schilly, M. M., Smith, R. B., Braile, L. W., & Ansorge, J. (1982). The 1978 Yellowstone-Eastern Snake River Plain Seismic Profiling Experiment: Data and upper crustal structure of the Yellowstone Region. Journal of Geophysical Research: Solid Earth, 87(B4), 2692-2704.

Shuey, R. T., Schellinger, D. K., Tripp, A. C., & Alley, L. B. (1977). Curie depth determination from aeromagnetic spectra. Geophysical Journal International, 50(1), 75-101.

Shuey, R. T., Schellinger, D. K., Johnson, E. H., & Alley, L. G. (1973). Aeromagnetics and the transition between the Colorado Plateau and Basin Range Provinces, Geology, 1, 107–110.

Sibson, R. H. (1974). Frictional constraints on thrust, wrench and normal faults. Nature, 249(5457), 542-544.

Smith, R. B., & Braile, L. W. (1982). Crustal structure and evolution of an explosive silicic volcanic system at Yellowstone National Park.

Smith, R. B., Jordan, M., Steinberger, B., Puskas, C. M., Farrell, J., Waite, G. P., Husen, S., Chang, W. L. & O'Connell, R. (2009). Geodynamics of the Yellowstone hotspot and mantle plume:

Seismic and GPS imaging, kinematics, and mantle flow. Journal of Volcanology and Geothermal Research, 188(1), 26-56.

Smith, R. B., Shuey, R. T., Freidline, R. O., Otis, R. M., & Alley, L. B. (1974). Yellowstone hot spot new magnetic and seismic evidence. Geology, 2(9), 451-455.

Smith, R. B., Sbar, M. L. (1974). Contemporary tectonics and seismicity of the western United States with emphasis on the Intermountain Seismic Belt, Geol. Soc. Amer. Bull., 85, 1205–1218.

Smith, R. B., Shuey, R. T., Pelton, J. R., & Bailey, J. P. (1977). Yellowstone hot spot: Contemporary tectonics and crustal properties from earthquake and aeromagnetic data. Journal of Geophysical Research, 82(26), 3665-3676.

Smith, R. B., & Arabasz, W. J. (1991). Seismicity of the Intermountain seismic belt.

Spector, A., & F. S. Grant, (1970). Statistical model for interpreting aeromagnetric data: Geophysics, 35, 2, 293–302.

Solaro, G., Tizzani, P., Milano, G., & Pauselli, C. (2007). Rheological behaviour of the crust in Southern Apennine (Italy): results from a thermal and seismological study. Terra Nova, 19(5), 353-359.

Stauffer, P. H. (2004). Tracking Changes in Yellowstone's Restless Volcanic System (No. 100-03).

Tanaka, A., Okubo, Y., & Matsubayashi, O. (1999). Curie point depth based on spectrum analysis of the magnetic anomaly data in East and Southeast Asia. Tectonophysics, 306(3), 461-470.

Tizzani, P., Battaglia, M., Castaldo, R., Pepe, A., Zeni, G., & Lanari, R. (2015). Magma and fluid migration at Yellowstone Caldera in the last three decades inferred from InSAR, leveling, and gravity measurements. Journal of Geophysical Research: Solid Earth, 120(4), 2627-2647.

Tselentis, G. A. (1991). An attempt to define Curie point depths in Greece from aeromagnetic and heat flow data. Pure and applied geophysics, 136(1), 87-101.

USGS, 1973, Aeromagnetic map of Yellowstone National Park and vicinity, Wyoming-Montana-Idaho: U.S. Geological Survey Open-File Report 73-304,4 sheets, scale 1:125,000.

Vasco, D. W., Smith, R. B., & Taylor, C. L. (1990). Inversion for sources of crustal deformation and gravity change at the Yellowstone caldera. Journal of Geophysical Research: Solid Earth, 95(B12), 19839-19856.

Vaughan, R. G., Keszthelyi, L. P., Lowenstern, J. B., Jaworowski, C., & Heasler, H. (2012). Use of ASTER and MODIS thermal infrared data to quantify heat flow and hydrothermal change at Yellowstone National Park. Journal of Volcanology and Geothermal Research, 233, 72-89.

Vazquez, J. A., & Reid, M. R. (2002). Time scales of magma storage and differentiation of voluminous high-silica rhyolites at Yellowstone caldera, Wyoming. Contributions to Mineralogy and Petrology, 144(3), 274-285.

Waite, G. P., & Smith, R. B. (2002). Seismic evidence for fluid migration accompanying subsidence of the Yellowstone caldera. Journal of Geophysical Research: Solid Earth, 107(B9).

White, D.E., Fournier, R.O., Muffler, L.J.P., & Trusdell, A.H. (1975). Physical results of research drilling in thermal areas of Yellowstone National Park, Wyoming: U.S. Geological Survey Professional Paper 892, 70 p.

White, D. E. (1969). Rapid heat-flow surveying of geothermal areas, utilizing individual snowfalls as calorimeters. Journal of Geophysical Research, 74(22), 5191-5201

Waite, G.P., Smith, R.B., 2004. Seismotectonics and stress field of the Yellowstone volcanic plateau from earthquake first motions and other indicators. J. Geophys. Res. 109, B02301.

Wicks, C., Thatcher, W., & Dzurisin, D. (1998). Migration of fluids beneath Yellowstone caldera inferred from satellite radar interferometry. Science, 282(5388), 458-462.

Wicks, C. W., Thatcher, W., Dzurisin, D., & Svarc, J. (2006). Uplift, thermal unrest and magma intrusion at Yellowstone caldera. Nature, 440(7080), 72